4.3 Monte Carlo with software signals

The event search algorithm should optimally detect a signal, built on a template with the same parameters of the filter, added to the input stream. This is the minimum request for the data analysis to be consistent, and it is sensitive to fast transient and spurious events. As a by-product it gives the empirical distributions for amplitude and timing errors, and for goodness-of-the-fit test statistic.

4.3.1 Introduction and implementation

While the best way to calibrate a bar detector for burst detection is of course to inject a mechanical pulse with calibrated amplitude, for certain purposes we do not need to actually disturb the system. In the rest of the section we assume that the system is perfectly linear (no cross-talks between signal and noise) and the transfer function is exactly known. Under these circumstances, we can perform a software version of the “kick and look” calibration procedures, which in the worse case is a null test, but can also point out interesting statistical parameters like biases in the timing error or the detection efficiency, whose scaling laws can be only roughly determined by theoretical calculations. The good of a software pulse is that as it is numerically added to the data it can also be exactly removed. And there is no limit in the number of pulses we can inject, apart from availability of computational time.

The software used to produce the following analysis is still test-type, and is not linked to the current stable release of the online analysis. It uses the filtered decimated data already archived to disk, which must preliminarily be resampled to about 5 kHz in order to apply the peak interpolation routine (see 4.1.3 for details).

The time stretch modified with the added SW pulse is taken long enough that its length plays no role in the results (see Figure 65). In practice, everything goes as the entire data stream was analyzed, with but one single pulse added each time.

In the following two paragraphs we shall give a demonstration of two different applications of this software tool.

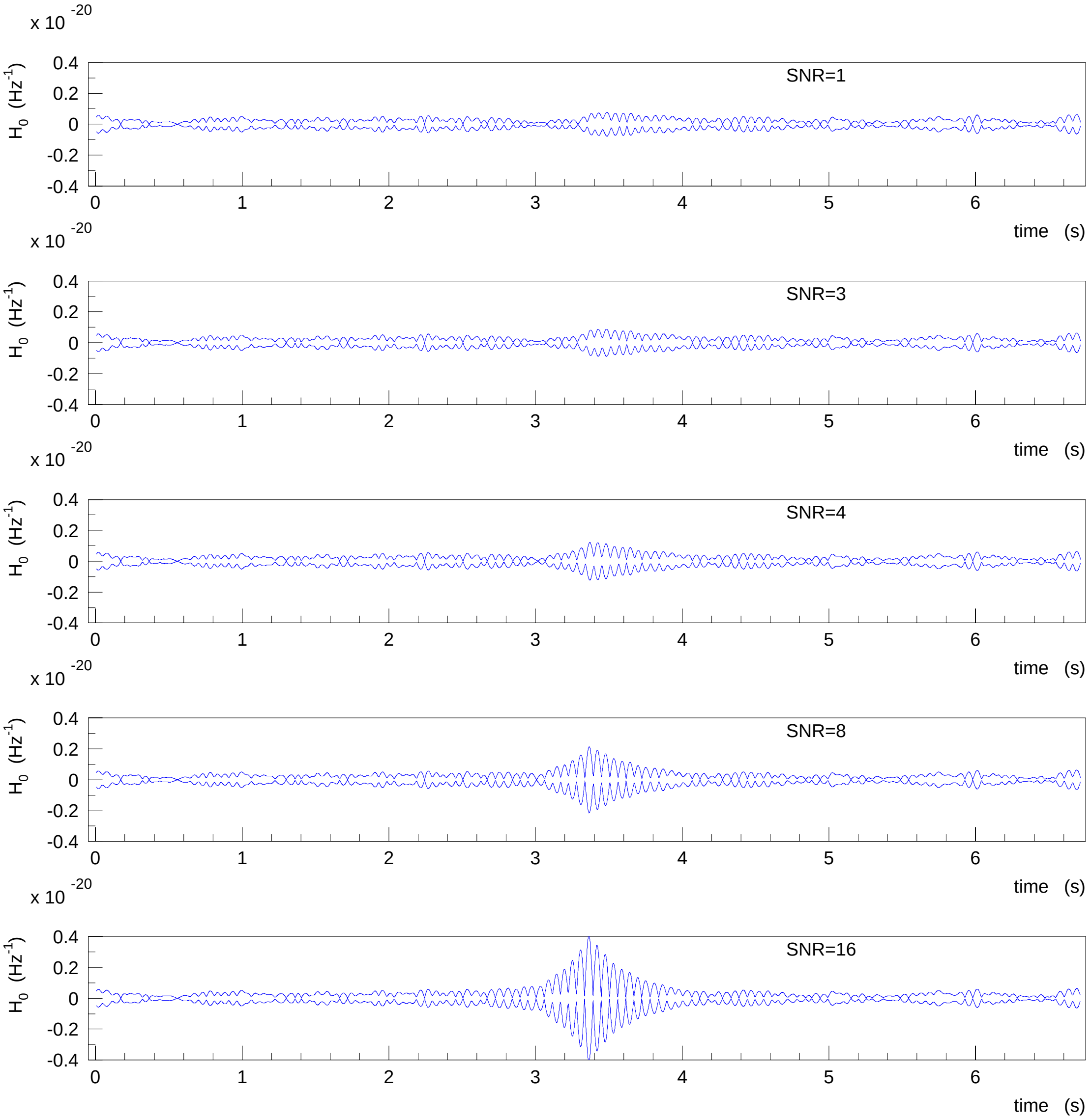

Figure 65. Appearence of a software added signal pulse (*SW-event*) in the filtered data after the peak interpolation routine, at various SNR's. The event injection time is in the middle of the buffer. The total duration of this stretch of data is set to 14 times the time constant of the filter, therefore the residual amplitude of the signal at the extremes is decayed of a factor 10^3.

4.3.2 Determining amplitude and timing error distributions

In this first example on a stretch of time lasting about one hour (UTC 1^h 4-Jul-1999) a series of SW events were sent regularly spaced at a constant rate of one per second, and cycling at each time step over a discrete set of absolute amplitudes, which were chosen so to span a range of SNR from 32 down to 1.

Have a look at Figure 66. What is happening at low SNR? Remember that event search is basically a nonlinear algorithm based on threshold crossing, which naturally enhances the extremes of the input stochastic process. If the signal dominates, the result is approximately equivalent to a linear problem and the estimated amplitude is a normal unbiased RV. When SNR≈2 nonlinear biases are showing up[22]. To see the problem in another way, we may point

[22] Even when there is no signal, SNR=0, the event search algorithm keeps producing full length event lists with amplitudes different than zero!

out that at such low SNR the background events are likely to dominate over the real ones (see Figure 71). The event amplitude would be just too low to be detected above any reasonable threshold, and when the latter starts to be *unreasonably* low then the greater noise fluctuations are picked up irrespective to the injected signal (which plays the role of a disturbance … to the noise itself!). These picked up events should in fact be properly considered *false alarms*.

The time error statistic at low SNR seems to confirm this reasoning. In Figure 67 (*a*,*b*) there is almost no sign of phase information, and the phase error appears scattered everywhere between 0 and 2π. The peak error in Figure 68 (*a*) appears very broadband, with just a small increase of the counts at zero delay. The broadband component in fact has two slowly decaying exponential queues (not shown in the figure), and this is exactly the behavior we expect with the procedure described above for a "null" signal. In fact, it should be remarked that the event search was not at all "blind", it was triggered by the a priori knowledge of the exact time of arrival of the pulse. Moreover there is a one to one correspondence to sent pulses and found events. Therefore, even with SNR=0 we expect the "nearest found" time error statistics to be Poissonian (i.e. exponential tailed density function), due to the random nature of the noise fluctuation extremes after decorrelation.

The conclusion from Figure 66, Figure 67 (*c*-*f*) Figure 68 (*c*-*f*) is that as long as the SNR is 4 or above, the amplitude deviates are modeled by a zero mean normal RV, and the variance of the amplitude error is an estimator of the variance of the underlying Gaussian stochastic process. The time error approaches the linear solution we anticipated in 1.3.3.

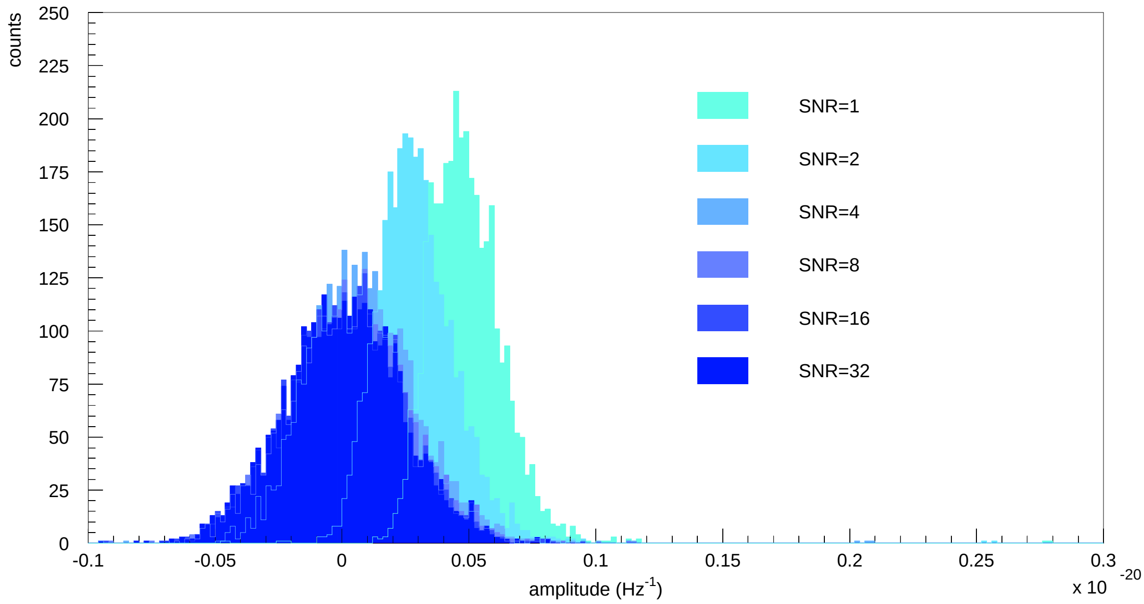

Figure 66. Histograms of the detected deviates of event amplitudes, when the event original amplitude is set at discrete levels, with a range of corresponding SNR's from 1 to 32. At high SNR the histograms reproduce the zero-mean Gaussian density function of the underlying gaussian stochastic noise. At SNR=2 the regime is manifestly no more linear, and a bias toward grater amplitudes appears.

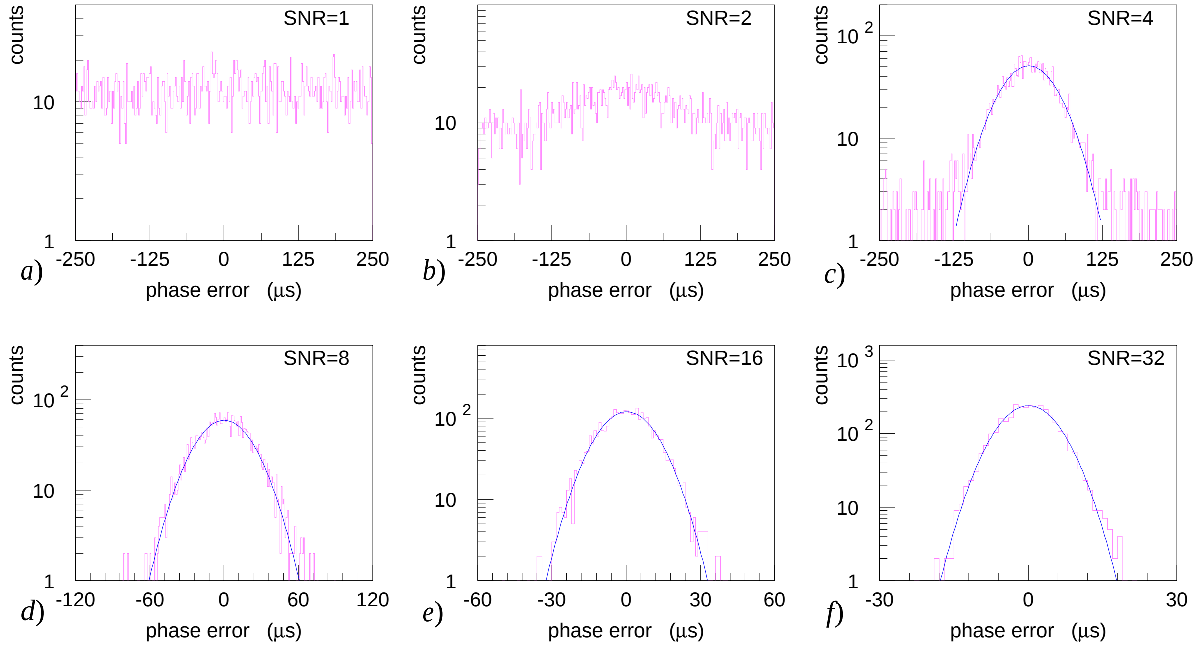

Figure 67 – (*above*) Phase error histograms relative to the example described in 4.3.2. Notice that ±270μs were the extremes values that the phase error could take. Therefore in (*a,b,c*) the abscissa spans almost the entire range of the phase error.

Figure 68 – (*below*) Peak error, expressed in integer number of peaks, for the example described in 4.3.2. Notice that in (*a,b,c*) are still clearly visible the side-peaks due to beat oscillations, while in (*d,e,f*) only the main lobe appears.

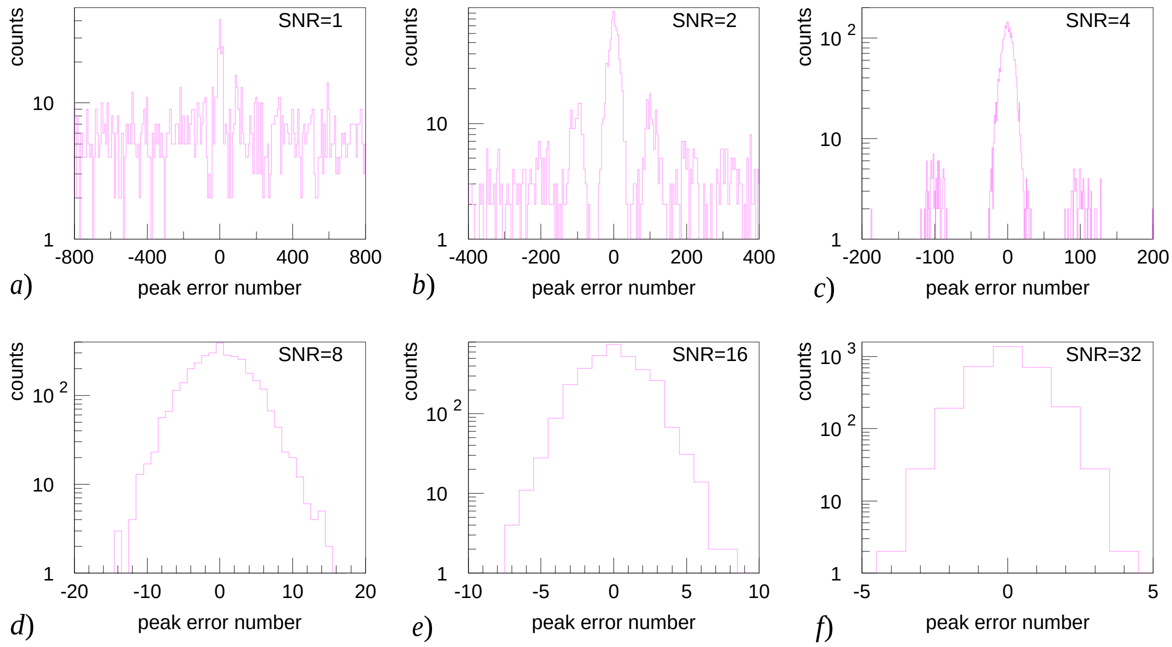

4.3.3 Determining the detection efficiency

To affirm the detection efficiency as a function of SNR at the 1‰ level we used 1 hour long time stretches. They are then subdivided in 20s time spans, like the sample shown in Figure 69 and Figure 70, 400 SW-events were sent with amplitudes packed between SNR=2 and SNR=12. Most of them were detected in the linear regime, and this gives us the ability of determine with a fair significance a few interesting statistical parameters, like the first few moments of the amplitude error density. Notice that recursive reasoning is implied, because we have first to determine with a coarse approximation what is the standard deviation of the amplitude noise, in order to select only results coming from *SNR* above 4. For the example discussed here, we stopped the recursion after one cycle.

We define within each 20s sample the "sent" signal-to-noise-ratio as the ratio of the original amplitude of the SW event and the mean square deviation of the measured amplitude. In a similar way we define the "detected" SNR using the final amplitude measured by our procedure. Finally, the estimator of the detection efficiency is defined as the ratio of the counted events over the total of SW events sent in a narrow SNR range. The results are shown in Figure 72.

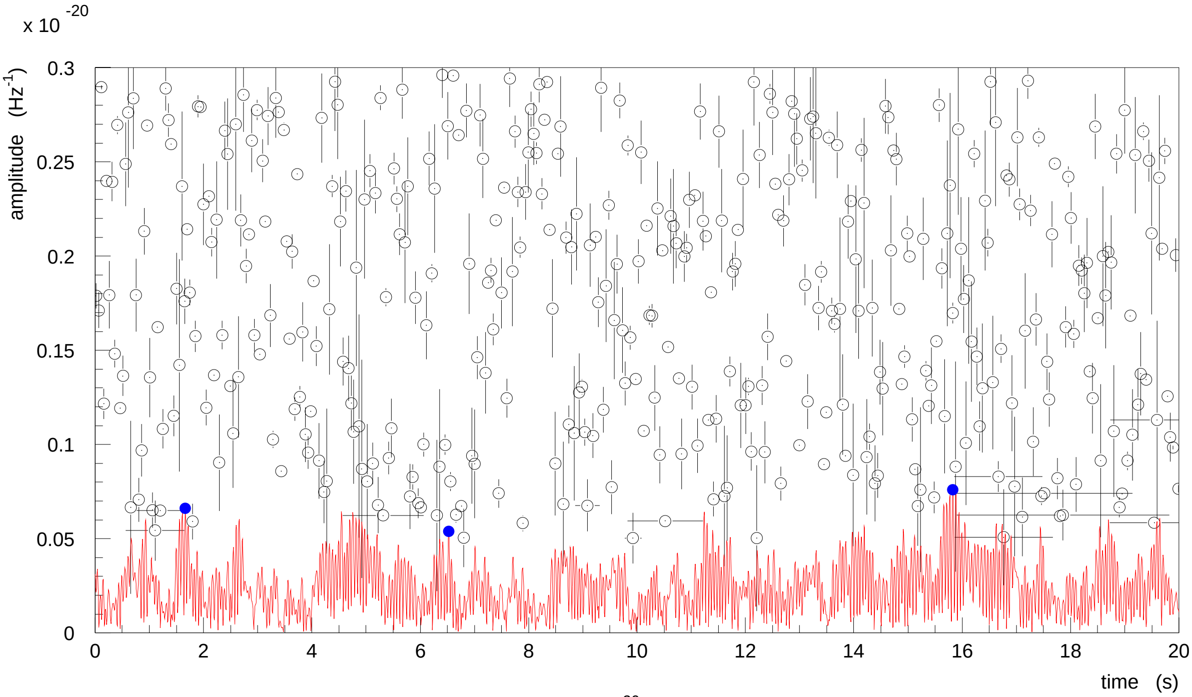

Figure 69. (*above*) A sample representation of 20 seconds of filtered data (200+220 from UTC 1h 4-Jul-1999) after the peak interpolation routine (positive vartical axis only). The blue spots represent the background events at the output of the event search algorithm. The empty circles target the initial time and amplitude of more or less randomly distributed software pulses, with original amplitude spanning from SNR as low as 2 to SNR=12. The vertical and orizontal bars are a measure of the time and amplitude displacement of detected SW events. It is noticeable that for a few very low SNR events the time displacement is huge, and you can see pretty well why: in each case a nearby fluctuation of the noise was slightly favoured by the decorrelation algorithm.

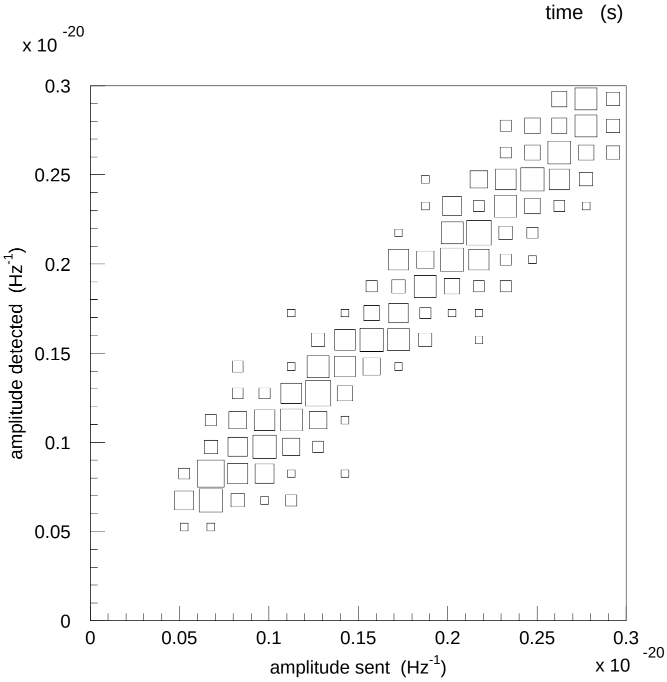

Figure 70. (*right*) a 2-dim histogram of measured vs original amplitude, for SW events of the same data sample illustrated in Figure 69. The plot correctly shows a linear dependence, with a constant vertical spread around the bisector.

Figure 71. Distribution of the background events collected in the same hour used for SW events demonstration below.

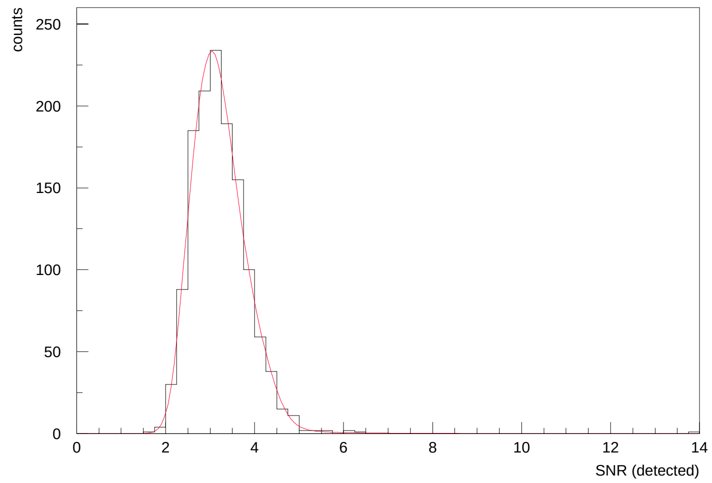

Figure 72. (*below*) Detection efficency as a function of the SNR and for a choice of different time windows. It is defined as the fraction of events recovered within a certain time window in a triggered coincidence search experiment. The two graphs differ because of the freedom in defining the SNR –either as it is detected naïvely by the observer or computed from the original signal amplitude. In the linear regime, when SNR>5 the results with either definition agree. The upward bending of the curves at low SNR is the symptome that false alarm probability is no more negligible. Vertical bars represent rms counting errors.

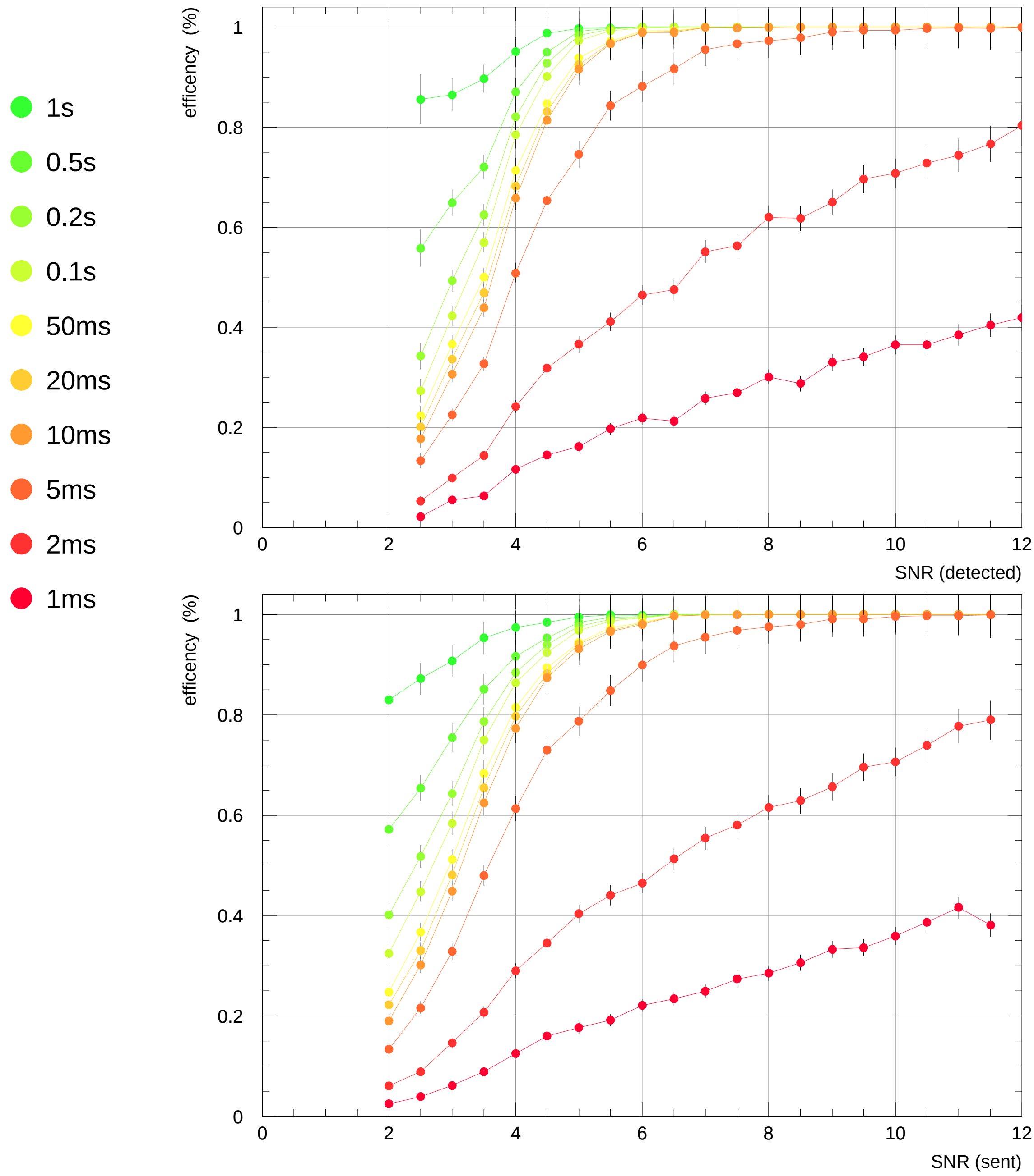

4.4 Data exchange protocol for coincidence and correlation analysis

4.4.1 Specifications

To summarize what we said in 3.1.1, there is a minimum of information that should be provided to proceed with coincidence analysis:

1. The time of arrival and amplitude of each candidate event;
2. The probability density function (pdf) for timing errors (random and systematic);
3. The pdf for amplitude errors (random and systematic);
4. The event search threshold.
5. The efficiency of the detection

To be useful in estimating upper limits correctly, information listed at 1÷5 should be given at each time, even when no event was detected or when the detector was not operating at all. The latter case could be handled by a conventional "∞" threshold or "0" efficiency.

A copy of the last IGEC data exchange protocol, now approved for its use in the next reprise of the data exchange, is included here for the reader's reference. New updated versions and instructions can be found in the Internet, at the page http://igec.lnl.infn.it/

IGEC-2000 protocol
version Dec. 4th

Pia Astone, Lucio Baggio, Paolo Bonifazi,
Giovanni A. Prodi, Antonello Ortolan

1. GENERAL STRUCTURE OF EXCHANGED FILES

The exchanged data of each detector are organized in **daily files** (0:00 – 24:00 Universal Time) with a name structured like the following example:

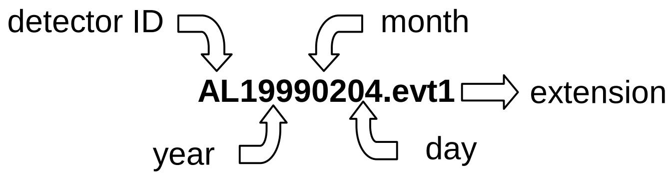

(AL=*ALLEGRO*, AU=*AURIGA*, EX=*EXPLORER*, NA=*NAUTILUS*, NI=*NIOBE*)
The file is written in standard **ASCII** format and its basic element is the **line**, which is made by a number of **fields** separated by **blank spaces**.
The files are made available to IGEC members by means of ftp sites with restricted access maintained by each group. In case an **update** of the already exchanged set of daily **files** is needed, the group involved will inform the partners and circulate within IGEC a document containing the description of the changes and their motivations; the superseded set of files will remain available in a different directory. The extension of a set of exchanged files will be *"evtn"* where n stands for the ordinal number of the set. Files are homogeneous only within a set (same extension) and the IGEC analysis will be based on the latest set of files available from each detector.
Each file contains a **declaration section** to give all the necessary information for data retrieving and a **data section** containing the exchanged data. A sample file is shown in appendix A.

DECLARATION SECTION

The following line types are mandatory:

- **Comments**
  Lines starting with "!" carry descriptive information in a human readable format. They should not carry information necessary for data retrieving or decoding.

  Sample line:

! Here starts the declaration section

- **Field declarations**
  Field declarations allow for a dynamic definition of the exchanged data. They describe the information carried by each field of exchanged data. A field declaration line starts with "#" followed by the code of the data line to

which it refers ("EVT", "VETO", "STATUS", "STOP","START"), the ordinal number of the field in the data line, the registered code of the field (implying both the physical quantity and its conventional units), the numeric variable type (I=integer, R=real, E=exponential).

Sample line:

#EVT 6 SEC R

The **registered codes** of the **fields** are summarized in *appendix B* for each data line

DATA SECTION:

- **Data lines**
  The fields in the data lines are the exchanged data. Each data line starts with "$" followed by its code. The mandatory lines and their functions are summarized here (see successive sections for details):
  $STATUS
  information on sensitivity of detector, threshold for event search
  $START
  beginning of "on" time of detector.
  $STOP
  beginning of "off" time of detector
  $EVT
  information on a candidate event for gw burst detection (δ-like signals)
  $VETO
  information on a vetoed event

  All lines are identified by a time and appear in **chronological order**.

  Sample line:

$STOP 1998 3 14 35 20.34

2. ALLOWED RATE OF CANDIDATE EVENTS

For each detector, the thresholds used for event search are set day by day depending on the detector noise in order to limit the maximum allowed rate of exchanged events according to the following requirement.
On the average, the **fraction of the observation time covered by the time error boxes of the exchanged events** of each detector **has to be upper bounded**:

$$\frac{\sum_i^{events} 2\delta t_i}{T_{obs}} \leq u.b.$$

where

- $\boldsymbol{\delta t_i = 2\,\sigma_t}$ i.e. twice the measured/calculated standard deviation of the time uncertainty of each event
- ***u.b.*** is now tentatively set to **0.5%** , but can be easily adjusted in the future to increase the rates of exchanged events
- $\boldsymbol{T_{obs}}$**= 1 day** because the requirement has to be met on a day by day basis (i.e. within each exchanged file).

3. SENSITIVITY, "on" and "off" TIME OF DETECTORS

The **mandatory $STATUS** line gives *all the relevant information on the detector operation* in terms of ***noise properties and false dismissal probability*** (sensitivity, amplitude uncertainty, threshold, etc.).
The **mandatory $STOP** line declares the end time of any effective observation of the detector.
The **mandatory $START** line declares the beginning time of any effective observation of the detector, with the requirement that *a $STATUS line be declared at the same time*.

- The **information** included in a **$STATUS** line is intended to be **valid until the next $STATUS** line or **$STOP** line or the end of the daily file, i.e. the variations of all the quantities are assumed to be neglegible from the declared date until the date of the successive $STATUS or $STOP line or the end of the daily file. ***It is mandatory to insert $STATUS lines at a rate suitable to meet this requirement.***
- **"on" and "off" times**. **$STOP** and **$START** lines are used as in the previous IGEC-1998 protocol and are mandatory to declare respectively the end and the beginning of any effective observation period of the detector. For each $START line, a corresponding *$STATUS line has to be declared at the same time* to provide the necessary information on the detector operation. Short interruptions of the observation of the detector due to transient disturbances are declared in the $VETO lines (see Sec. 5.). ***The data section of any exchanged daily file has to begin with a $STATUS line***.[1]

The following **fields are mandatory** in the **$STATUS** line
- ***date*** fields in Universal Time: year, month, day, hour, minutes (field codes: YEA, MON, HOU, MIN; integers) and seconds-and-fractions (SEC; real).
- ***threshold*** used by the event search algorithm in terms of the Fourier component H of the strain gw amplitude h (THR; units Hz^{-1}). Its value has to be corrected for any known bias on the estimate of H (as, for instance, due to the filter)**.**
- ***relative systematic uncertainty on amplitude*** of the detector (SYS, pure real number) as due to calibration errors and biases because of mismatches of data filtering parameters. The relative uncertainty will be ± (value of the field).

[1] To ensure that each file be self-consistent, there must be a $STATUS line describing the operation of the detector (sensitivity, threshold, …) prior to any other data line. In this way there is no need to look back in previous files. For instance, in case the detector is "on" from the previous day, a $STATUS line with time hour=0, min=0, sec=0.0 has to be given as the first line of the data section. In case the detector is "off" before and at hour=0, min=0, sec=0.0 , the first lines of the data section have to be a $START and a $STATUS line, whose date will be the beginning of a new "on" time. Two exceptions of the rule "the data section has to begin with a $STATUS line" are possible: 1) the data section itself is empty (detector "off" for the entire day) or 2) there is a $STOP line at hour=0, min=0, sec=0.0.

- ***detector amplitude noise*** in terms of **square root of the variance** (σ_H) of the distribution of **amplitude** estimates (MA2, units Hz^{-1}).

*It is **recommended** to provide as well the following additional fields in the **$STATUS** line:*

- *the **3^{rd}** and **4^{th}** order **central moments** of the distribution of **amplitude estimates** relative to σ_H , that is divided by σ_H^3 and σ_H^4 respectively (MA3, MA4, real, pure numbers).*
- *the **live time** fraction of the detector, that is the fraction of the time ending with the next $STATUS line during which the detector has not been blinded by all the registered events, both good candidates and vetoed ones (LIV, real, pure number). As an alternative, it is recommended to supply the duration of each event in the $EVT line.*

Sample of a $STATUS line
showing the mandatory fields

relative systematic uncertainty

$STATUS 1998 12 25 12 0 3.02 1.55E-21 0.1 ···

date

threshold

··· 0.31E-21 + non-mandatory fields[2]

σ_H

The following **fields are mandatory** in the **$STOP** and **$START** lines

- ***date*** fields in Universal Time: year, month, day, hour, minutes (field codes: YEA, MON, HOU, MIN; integers) and seconds-and-fractions (SEC, real).

[2] AURIGA and ROG would include MA3 and MA4

4. CANDIDATE EVENTS

The **mandatory $EVT** line gives ***all the relevant information which is specific to an event considered good candidate for gw burts detection*** (transient signal with flat Fourier spectrum over the frequency bandwidth of detection)***.***

The following **fields are mandatory** in the **$EVT** line

- ***date*** fields in Universal Time give the estimated arrival time of the event as year, month, day, hour, minutes (field codes: YEA, MON, HOU, MIN; integers) and seconds-and-fractions (SEC, real). The arrival time has to be corrected for any known bias as due to synchronization etc..
- ***time uncertainty*** in terms of **square root of the variance** (σ_t) of the distribution of the estimates of the arrival time of the event (field code: MT2, units sec).
- ***amplitude*** of the candidate event in terms of the Fourier component H (AMP, units Hz^{-1}) of the gw amplitude h. The amplitude is estimated by a filter matched to a δ-like gw signal (gw burst) and is required to be **unbiased**. The information on amplitude uncertainty to be used in the IGEC analyses is declared in the previous $STATUS line.

*It is **recommended** to provide as well the following additional fields in the **$EVT** line:*

- *the **3rd** and **4th** order **central moments of the statistical uncertainty on arrival time** relative to σ_t , that is divided by σ_t^3 and σ_t^4 respectively (MT3, MT4, real, pure numbers).*
- *the **time duration** of the event as seen by the algorithm used to search for events in the filtered data (DUR, units sec)[3] together with the corresponding **time delay** of the event with respect to the beginning of its time duration (DT, units sec). As an alternative, it is recommended to supply the live time fraction in the $STATUS line.*

Sample of a $EVT line

showing the mandatory fields

σ_t

$EVT 1998 12 25 12 0 3.02 0.37 1.55E-21 +

event time

amplitude

+ non-mandatory fields[4]

---

[3] The time duration is the time span around an event during which the event search algorithm cannot resolve another event. In case of AURIGA, it is set to a certain number of the typical time of the filter (currently it is fixed to 6 Wiener times). In case of ROG, it is the time during which the amplitudes of the oscillations of the filtered data stay above a selected threshold (currently SNR=3.8) plus a fixed time (currently 1 sec) after its down threshold crossing (to be more precise, after the first the down threshold crossing which is not followed by an up threshold crossing within the cited fixed time).

[4] AURIGA would include MT3, MT4, CHI, DOF, DUR, DT

A **general recommendation** has to be made: the ***event search algorithms should intrinsically ensure a suitable separation of successive events*** with respect to typical time error boxes (for instance $> 2 \times (\sigma_{t,i} + \sigma_{t,i+1})$. In case two successive events in a file be in "self-coincidence", the IGEC analyses will define how to "merge" these events.

Other registered non mandatory fields for $EVT line:

- **SNR**: the signal-to-noise ratio of the amplitude of the event (AMP/σ_H)
- **CHI** : reduced chi-square of the event with respect to the expected shape of a δ-like gw burst with **DOF** (number of degrees of freedom)
- **MA2**: another different estimate of σ_H (notice however that the σ_H to be used in IGEC analyses is understood to be the one included in the previous $STATUS line)
- …

ROG would include MA2, SNR, DUR, DT,

5. VETOED EVENTS and TRANSIENT DISTURBANCES

In the **$VETO** line it is **mandatory** to declare each **event** or transient disturbance **not to be considered a good candidate for gw burst search** and vetoed by internal criteria set by each group. These vetoed events are intended to be used for diagnostic purposes only (for instance to look for any correlation among detector disturbances and to define short interruptions of the observation of the detector).

The following **fields are mandatory** in the **$VETO** line

- ***date*** fields in Universal Time give the estimated arrival time of the vetoed event as year, month, day, hour, minutes (field codes: YEA, MON, HOU, MIN; integers) and seconds-and-fractions (SEC, real).
- *total **time duration*** of the vetoed event as seen by the algorithm used to search for events in the filtered data (field code DUR, units sec) and the corresponding ***time delay*** of the event time with respect to the beginning of its time duration (DT, units sec).

*It is **recommended** to provide as well additional fields in the **$VETO** line:*

- ***amplitude** of the vetoed event as estimated by the filter for δ-like signals (AMP, units Hz^{-1}). Notice that this estimate is likely to be biased.*
- ***type** of internal veto applied by the group (TYP, integer).* The possible causes *of a veto are one or more of the following:*

0) χ^2 test failure
1) coincidence with mechanical ambient disturbance (seismic, vibrational, acoustic …)
2) coincidence with electromagnetic ambient disturbance
3) coincidence with cosmic ray
4) coincidence with disturbances in the front end electronics (gain fluctauations…)
5) coincidence with direct action of experimentalists (switching on instrumentation, calibration pulse …)
6) event of too long duration
7) others (to be specified if needed).

The value of the veto type is the integer $\sum_{i=0}^{3} n_i 2^i$, where $n_i = 0,1$ is a flag indicating if the i^{th} veto type of the previous list is (1) or not (0) involved. For instance the value "5" (binary 00001001) *would correspond to an event failing the χ^2 test and in coincidence with an electromagnetic disturbance.*

Sample of a $VETO line
showing the mandatory fields

time duration ←   → time delay

$VETO $\underbrace{\texttt{1998 12 25 12 0 3.02}}_{\text{event time}}$ 2.17 1.08 +

+ non-mandatory[5]

[5] AURIGA would include TYP, AMP
ROG would include AMP

Appendix A

sample template of file, to be substituted by a regular true file when available

```
! sample template of the declaration section , only the mandatory fields are declared here
#EVT 1 YEA I
#EVT 2 MON I
#EVT 3 DAY I
#EVT 4 HOU I
#EVT 5 MIN I
#EVT 6 SEC R
#EVT 7 MT2 R
#EVT 8 AMP R
#STATUS 1 YEA I
#STATUS 2 MON I
#STATUS 3 DAY I
#STATUS 4 HOU I
#STATUS 5 MIN I
#STATUS 6 SEC R
#STATUS 7 THR R
#STATUS 8 SYS R
#STATUS 9 MA2 R
#VETO 1 YEA I
#VETO 2 MON I
#VETO 3 DAY I
#VETO 4 HOU I
#VETO 5 MIN I
#VETO 6 SEC R
#VETO 7 DUR R
#VETO 8 DT R
#START 1 YEA I
#START 2 MON I
#START 3 DAY I
#START 4 HOU I
#START 5 MIN I
#START 6 SEC R
#STOP 1 YEA I
#STOP 2 MON I
#STOP 3 DAY I
#STOP 4 HOU I
#STOP 5 MIN I
#STOP 6 SEC R
! sample template of data section, not true data
$STATUS 1998 4 29 0 0 0.0 5.2E-21 0.15 1.5E-21
$EVT 1998 4 29 0 23 7.53 0.37 0.5.21E-21
$STOP 1998 4 29 0 26 0.0
$START 1998 4 29 23 2 0.0
$STATUS 1998 4 29 23 2 0.0 4.8E-21 1.385E-21
$EVT 1998 4 29 23 3 59.02 0.24 6.2E-21
$VETO 1998 4 29 23 34 15.67 2.24 1.12
$EVT 1998 4 29 23 34 23.87 0.38 4.8E-21
$STATUS 1998 4 29 23 37 41.0 5.02E-21 0.15 1.45E-21
$EVT 1998 4 29 23 37 53.46 0.38 5.04E-21
$EVT 1998 4 29 23 38 8.69 0.16 1.1E-20
$EVT 1998 4 29 23 58 25.21 0.38 5.02E-21
! eof, ciao, bye
```

Appendix B

Summary of the **registered field codes** for each data line. Any field code should be registered here to avoid ambiguities among exchanged files from different groups.

Field code	Numeric variable type	units	description	Related data lines
AMP	E, R	Hz^{-1}	Amplitude of event/disturbance	\$EVT \$VETO
CHI	R, E		Chi-square of event	\$EVT
DAY	I	d	Day of UTC date	\$START, \$STOP \$STATUS \$EVT \$VETO
DOF	R, E		Number of degrees of freedom of chi-square of event	\$EVT
DT	R, E	sec	Time delay of event/disturbance time with respect to its beginning	\$EVT \$VETO
HOU	I	h	Hour of UTC date	\$START, \$STOP \$STATUS \$EVT \$VETO
MIN	I	min	Minutes of UTC date	
MON	I	month	Month of UTC date	
MA2	R, E	Hz^{-1}	Standard deviation of filtered amplitude	\$STATUS \$EVT
MA3	R, E		3^{rd} central moment of filtered amplitude normalized by $MA2^3$	
MA4	R, E		4^{th} central moment of filtered amplitude normalized by $MA2^4$	
MT2	R, E	sec	Standard deviation of event time error	\$EVT
MT3	R, E		3^{rd} central moment of event time error normalized by $MT2^3$	
MT4	R, E		4^{th} central moment of event time error normalized by $MT2^4$	
SEC	R, E	sec	Seconds of UTC date	\$START, \$STOP \$STATUS \$EVT \$VETO
SNR	R, E		Signal-to-noise ratio in amplitude	\$EVT
SYS	R, E		Relative systematic error on amplitude estimates	\$STATUS
THR	E, R	Hz^{-1}	Threshold used for the event search	\$STATUS
TYP	I		Type of veto applied to the event	\$VETO
YEA	I	yr	Year of UTC date	\$START, \$STOP \$STATUS \$EVT \$VETO

5 Appendix

χ^2 testing of optimal filters for gravitational wave signals: An experimental implementation

L. Baggio and M. Cerdonio
Dipartimento di Fisica, Università di Padova and INFN, Sezione di Padova, via Marzolo 8, 35100 Padova, Italy

A. Ortolan and G. Vedovato
INFN, Laboratori Nazionali di Legnaro, via Romea 4, 35020 Padova, Italy

L. Taffarello and J.-P. Zendri
INFN, Sezione di Padova, via Marzolo, 8, 35100 Padova, Italy

M. Bonaldi and P. Falferi
CeFSA, Centro ITC-CNR, Trento and INFN, Gruppo Collegato di Trento, 38050 Povo, Trento, Italy

V. Martinucci, R. Mezzena, G. A. Prodi, and S. Vitale
Dipartimento di Fisica, Università di Trento and INFN, Gruppo Collegato di Trento, 38050 Povo, Trento, Italy

(Received 16 November 1999; published 14 April 2000)

We have implemented likelihood testing of the performance of an optimal filter within the online analysis of AURIGA, a sub-Kelvin resonant-bar gravitational wave detector. We demonstrate the effectiveness of this technique in discriminating between impulsive mechanical excitations of the resonant-bar and other spurious excitations. This technique also ensures the accuracy of the estimated parameters such as the signal-to-noise ratio. The efficiency of the technique to deal with nonstationary noise and its application to data from a network of detectors are also discussed.

PACS number(s): 04.80.Nn, 02.60.Ed, 95.55.Ym, 95.75.−z

I. INTRODUCTION

The Wiener-Kolmogoroff (WK) optimal filter is the main tool of signal extraction for gravitational wave (GW) detectors. In Gaussian noise, WK filtering is fully equivalent to maximum likelihood fitting of a signal model to the data. As a consequence, hypothesis testing can be applied to the filter by means of a proper sufficient statistics, as is the case for any other maximum likelihood fit. We have shown recently [1] that, in the presence of pure Gaussian noise, a likelihood hypothesis test leads to a standard χ^2 test of the ''goodness of the fit.'' These ideas have been implemented within the data analysis of the AURIGA ultracryogenic detector [2].

We performed a preliminary bench test of our filtering and event discrimination algorithms by using a room temperature resonant-bar detector. We then applied the algorithms to the AURIGA detector as soon as it started taking data in June 1997. In this paper, we report on the performance of the method and on the procedures we use to cope with the problem of the noise being nonstationary and non-Gaussian.

The paper is organized as follows. In Sec. II we summarize the theory of χ^2 test in the framework of WK filtering theory. In Sec. III we draw our model for the detector transfer function and noise spectrum. The experimental setup both for the room temperature test facility and for the cryogenic detector is reviewed in Sec. IV. Section V is devoted to the practical implementation of the WK filter, and results of χ^2 event characterization are reported in Sec. VI. Finally, in Sec. VII we discuss the relevance of this technique to the case of a single detector and of a network of gravitational wave (GW) detectors.

II. SIGNAL ANALYSIS AND HYPOTHESIS TESTING

A simplified model for a GW detector is that of a linear system with an output noise $n(t)$, which is commonly described as a stationary stochastic process with Gaussian statistics. In the following of this section we adopt a discrete time domain representation, that is we substitute for $n(t)$, a finite length sequence of samples $n_i \equiv n(i\Delta t)$. In this way we get a set $\{n_i\}$ of Gaussian random variables (GRV), with $0 \leqslant i \leqslant N$.

If a signal enters the system at time t_0, the sampled output of the detector is $x_i = \mathrm{A} u_i(t_0, \vartheta_j) + n_i$, where $\{u_i\}$ is the properly normalized signal template, A its amplitude and $\{\vartheta_j\}$ any other parameter set the signal may depend on.

A well established result [3] of signal analysis states that the minimum variance, unbiased linear estimate of the amplitude A is the GRV:

$$\hat{A} = \frac{\Sigma_{ij}\mu_{ij}u_i x_j}{\Sigma_{hk}\mu_{hk}u_h u_k} \equiv \sigma_{\hat{A}}^2 \cdot \sum_{ij} \mu_{ij} u_i x_j \equiv \sum_j w_j x_j, \tag{1}$$

if one assumes to know u, t_0, ϑ_i and the inverse cross correlation function μ_{ij} of the noise. Here the w_j's are then the coefficients of the WK filter matched to the signal $\{u_i\}$ and $\sigma_{\hat{A}}^2$ is the variance of $\hat{A}$

$$\sigma_{\hat{A}}^2 = \frac{1}{\Sigma_{hk}\mu_{hk}u_h u_k}. \tag{2}$$

When the noise has Gaussian statistics, the WK filter happens to be also a maximum likelihood estimator. In fact, the likelihood function associated with the data set $\{x_i\}$ is

$$\Lambda(x_1,x_2,\ldots;A)\propto\exp\left[-\frac{1}{2}\sum_{ij}\mu_{ij}(x_i-Au_i)(x_j-Au_j)\right], \tag{3}$$

where the sum runs over the number of data N. It is straightforward to verify that Λ reaches its maximum value for A equal to the value given by Eq. (1).

For this same value, the log-likelihood ratio

$$X\equiv\sum_{ij}\mu_{ij}(x_i-\hat{A}u_i)(x_j-\hat{A}u_j) \tag{4}$$

reaches a minimum.

It can be easily shown that X in Eq. (4) is a random variable with a standard χ^2 statistics. By performing the transformation $\{y_i\equiv\Sigma L_{ij}x_j\}$, where L is the *whitening* filter that diagonalize $\mu_{ij}(L^{-1}_{mi}\mu_{mn}L^{-1}_{nj}=\delta_{ij})$, one gets

$$X\equiv\sum_{i}(y_i-\hat{A}v_i)^2, \tag{5}$$

with $\{v_i\equiv\Sigma L_{ij}u_j\}$. This is the linear least square sum for a standard fit of the function $\{v_i\}$ to the data $\{y_i\}$ which is well known to be χ^2 distributed with $N-1$ degrees of freedom and to be independent of $\hat{A}$.

In order to evaluate X, it is easier to work with the equivalent expression [1]:

$$X=\left[\sum_{ij}\mu_{ij}x_ix_j-\frac{\hat{A}^2}{\sigma^2_{\hat{A}}}\right]=\left[\sum_{i}y_i^2-\frac{\hat{A}^2}{\sigma^2_{\hat{A}}}\right]. \tag{6}$$

Equation (6) shows that if the n parameters t_0 and $\{\vartheta_i\}$ are also unknown, their maximum likelihood estimate is the one that makes $\hat{A}^2/\sigma^2_{\hat{A}}$ a maximum. This is in general a non linear fit, and the resulting X is distributed as a χ^2 with $N-n-1$ degrees of freedom but only within a linear approximation.

We will use in the following mostly the reduced experimental $\chi^2_a\equiv[1/(N-n-1)]X$ which is expected to be distributed as a reduced chi-square χ^2_r. This statistic has unitary mean value for any number of degrees of freedom $N-n-1$.

The χ^2_a can be used as a statistical test of goodness-of-the-fit. It can be used to test for consistency of *a priori* hypothesis on the signal template $\{u_i\}$, with probability thresholds given either by theoretical predictions or by Monte Carlo simulations for the nonlinear case.

It is worth pointing out that, if a set of data fails the test, the resulting estimates for the amplitude $\hat{A}$ and for the other parameters are, in principle, biased. In this sense, the test appears as an unavoidable step of the overall filtering procedure. The relation between the bias on the amplitude estimate and the value of X can be determined analitically. We already pointed out [4] that, if data contain a signal $\{f_i\}$ different from that $\{v_i\}$ to which the filter has been matched, the experimental value of X fluctuates around a mean value proportional to the square of the signal-to-noise-ratio SNR $\equiv\hat{A}/\sigma_{\hat{A}}$. In the rest of this section we will work on the whitened data, and the signal $\{f_i\}$ and the template $\{v_i\}$ are referred at the output of the whitening filter. The apparent chi-square statistics is

$$\chi^2_a=\chi^2_r+\frac{1}{N-n-1}\{(\mathrm{SNR}^f_o)^2-(\mathrm{SNR}^v_o)^2+2(\mathrm{SNR}^f_o\mathrm{SNR}^f_n-\mathrm{SNR}^v_o\mathrm{SNR}^v_n)\}, \tag{7}$$

where SNR^f_o is the mean value of the signal to noise ratio for the signal $\{f_i\}$ with a filter matched to it, and SNR^v_o is that with the filter matched to $\{v_i\}$. SNR^f_n and SNR^v_n are their fluctuating parts, i.e., two Gaussian random variable with zero mean value and unit variance.

The mean value of χ^2_a is then

$$\langle\chi^2_a\rangle=\langle\chi^2_r\rangle+\frac{1}{N-n-1}\langle(\mathrm{SNR}^f_o)^2-(\mathrm{SNR}^v_o)^2\rangle=1+\lambda(\mathrm{SNR}^v_o)^2, \tag{8}$$

where

$$\lambda=\frac{\sum_{i=1}^{N}f_i^2\sum_{i=1}^{N}v_i^2-\left(\sum_{i=1}^{N}f_iv_i\right)^2}{(N-n-)\left(\sum_{i=1}^{N}f_iv_i\right)} \tag{9}$$

is a value that reduces to zero if $f_i=v_i$. Notice that λ is proportional to the square of the bias on the signal-to-noise ratio due to the filter inaccuracy.

III. WK FILTER FOR MODELED GW RESONANT DETECTORS

A resonant-bar detector coupled to a capacitive electromechanical transducer can be quite accurately modeled by an equivalent lumped elements electrical circuit [5]. It is easy to show that the transfer matrix between any port within the circuit and the readout port, always contains the same series of M poles, the kth pair of complex conjugate poles corresponding to a normal oscillation mode with frequency ω_k and quality factor Q_k. The noise generated by any generator within the circuit is transferred to the output through one of these transfer matrices. The total output noise results from the sum of these contributions plus the wide band noise S_0 of the final amplifier. It is easy to calculate that, with these assumptions, the total output noise spectral density is

$$S(\omega)=S_0\prod_{k=1}^{M}\frac{(i\omega-q_k)(i\omega+q_k)(i\omega-q_k^*)(i\omega+q_k^*)}{(i\omega-p_k)(i\omega+p_k)(i\omega-p_k^*)(i\omega+p_k^*)}, \tag{10}$$

where $p_k = i\omega_k - \omega_k/(2Q_k)$ and where the complex zeros q_k's are related to the optimal bandpass WK filter.

$S(\omega)$ possesses a few key features. First, the degrees of the polynomials appearing in the numerator and in the denominator are equal, a consequence of having modeled the wide band noise S_0 as purely white. Secondly, poles and zeros appear in pairs $\pm p_k$ and $\pm q_k$, as the noise spectral densities are transferred through the square modulus of transfer functions. Finally, as already mentioned, for each pole (or zero) its complex conjugate also appears, a consequence of reality of circuit elements.

The transfer function for an input GW delta pulse will contain the same poles $\{p_k\}$. Reality imposes then that the output signal $u_\delta(t)$ has a Fourier transform $\tilde{u}_\delta(\omega)$ given by

$$\tilde{u}_\delta(\omega) = \frac{\prod_{j=1}^{\tilde{M}} (i\omega - r_j)(i\omega - r_j^*)}{\prod_{k=1}^{M} (i\omega - p_k)(i\omega - p_k^*)}, \tag{11}$$

with $M > \tilde{M}$ because of the stability of the system and where the coefficients r_i are obviously the zeroes of the function.

It is well known that the continuous version of the WK filter function, $w(t)$, has a Fourier transform $\tilde{w}(\omega) = \sigma_{\hat{A}}^2 S^{-1}(\omega)\tilde{u}_k^*(\omega)$. By using Eqs. (10) and (11) one gets, for $\tilde{w}(\omega)$,

$$\tilde{w}(\omega) = \sigma_{\hat{A}}^2 S_0^{-1} \frac{\prod_{j=1}^{\tilde{M}} (i\omega + r_j)(i\omega + r_j^*)}{\prod_{k=1}^{M} (i\omega + q_k)(i\omega + q_k^*)} \times \prod_k \frac{(i\omega - p_k)(i\omega - p_k^*)}{(i\omega - q_k)(i\omega - q_k^*)}. \tag{12}$$

The WK filter splits up in the product $L(\omega)M(\omega)$, where

$$L(\omega) = S_0^{-1/2} \prod_k \frac{(i\omega - p_k)(i\omega - p_k^*)}{(i\omega - q_k)(i\omega - q_k^*)} \tag{13}$$

is the *whitening filter* for the noise with PSD $S(\omega)$. This means that a filter with transfer function $L(\omega)$ produces at its output a noise with spectral density $S_w = 1$ when fed at the input with the detector noise with PSD $S(\omega)$, because $|L(\omega)|^2 S(\omega) = 1$.

$M(\omega)$ is defined by

$$M(\omega) = \sigma_{\hat{A}}^2 S_0^{1/2} \frac{\prod_{j=1}^{\tilde{M}} (i\omega + r_j)(i\omega + r_j^*)}{\prod_{k=1}^{M} (i\omega + q_k)(i\omega + q_k^*)}. \tag{14}$$

It is a bandpass filter around the frequencies $\omega_k \equiv |\mathrm{Im}(q_k)|$ with bandwidths $\Delta\omega_k^{\mathrm{opt}} \equiv 2|\mathrm{Re}(q_k)|$ which are usually much larger than $\Delta\omega_k \equiv 2|\mathrm{Re}(p_k)| = \omega_k/Q_k$.

Most of the information needed to process the data is contained within this filter matched to a delta-shaped pulse. The response of the system to any other input signal $h(t)$ can always be written as the time convolution $u_\delta * h$, so that, once data have been filtered with the optimum filter matched to u_δ, one can perform the complete WK filtering for $h(t)$ by a simple convolution of $h(t)$ with the filtered data.

In addition, it turns out that for resonant detectors most of the expected signals have Fourier transforms that are rather flat across the comparatively small post filtering bandwidths ($\sim$1 to 10 Hz) of the detectors, and are thus indistinguishable from a delta pulse [6].

One can show that, for the case of a resonant-bar detector with resonant transducers, in Eq. (14), $M = 2$, $\tilde{M} = 1$ and $r_1 = 0$. As a consequence, the band-pass filter $M(\omega)$, which is purely anticausal, introduces an anticausal component in the response and cannot be implemented in real time.

In addition, the sets $\{p_k\}$ and $\{q_k\}$, along with S_0, are the only relevant parameters that enter both the noise spectrum and the transfer function of the system. As a consequence, a check that the PSD of the whitened data is indeed flat within its statistical error, becomes a very useful consistency test for the accuracy of the filter. In Sec. V we show how we feed back the deviation from a white spectrum to an automatic adaptive procedure that updates the values of filter parameters.

IV. EXPERIMENTAL LAYOUT

The AURIGA detector [2] consists of a 2.3 tons, 3 m long A15056 bar equipped with a capacitive electromechanical transducer and a dc superconducting quantum interference device (SQUID) preamplifier. The bar hangs on a multiple stage pendulum attenuation system (-240 db at 1 kHz), kept at 0.2 K by a ^{3}He-^{4}He dilution refrigerator. The signal is acquired by an analogue to digital converter (ADC) at 4.9 kHz and synchronized to UTC by means of a Global Positioning System (GPS) clock [7] (see Fig. 1).

The room temperature detector used for some of the tests shares almost all the relevant features with the cryogenic detector. The most noticeable difference, besides the absence of the cooling system, is that the voltage across the capacitive transducer is fed to very low noise field effect transistor (FET) preamplifier.

As far as signal analysis is concerned, the most relevant differences among the two detectors are the Q factors ($\approx 10^4$ for the room temperature detector and slightly larger than 10^6 for AURIGA) and the post filtering bandwidth $\Delta\omega_k^{\mathrm{opt}}$ (corresponding to $\approx$10 Hz for the room temperature detector and $\approx$1 Hz for AURIGA).

The room temperature detector mounts an electromechanical capacitive actuator, a detuned version of the transducer, placed on the face opposite to the one used to extract the signal. It provides a way to excite the bar with short mechanical bursts that mimic a GW signal.

In order to test the χ^2 performance for spurious excita-

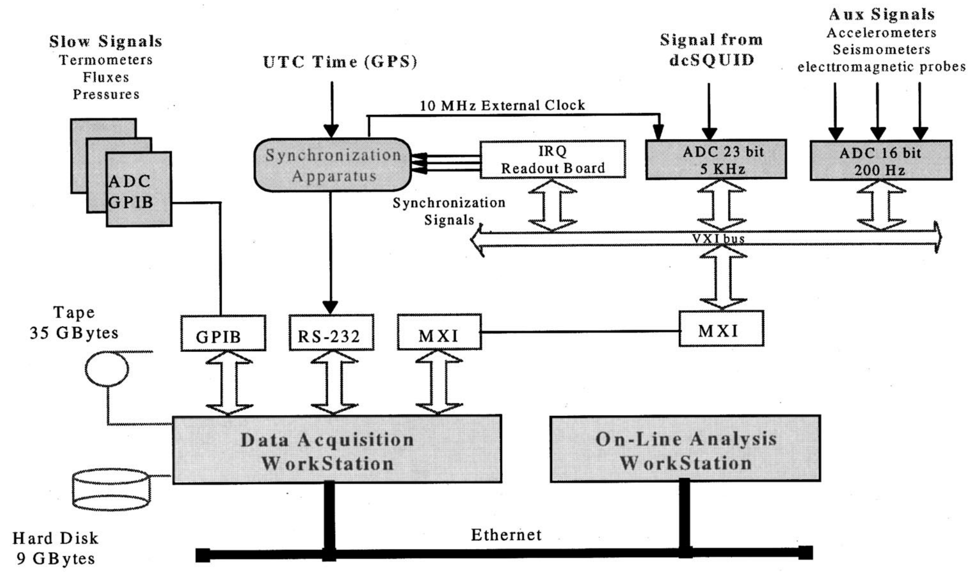

FIG. 1. Schematic drawing of the AURIGA data acquisition system. The signal channel from the transducer and dc SQUID amplifier system is acquired by the 23 bit ADC at about 4.9 kHz. The synchronization with UTC of the acquired data is achieved in hardware well within 1 μs by dedicated interrupts and triggers between the ADC and a GPS clock with a stabilized local oscillator. The full raw data are then fully archived and analyzed on-line.

tions due to electrical disturbances, short current pulses were injected into a coil inductively coupled to the amplifier-input leads. These pulses were also used to trigger data acquisition as described in Ref. [8].

V. DATA ANALYSIS AND χ^2 EVALUATION

The on-line analysis of the AURIGA detector has been described elsewhere [7]. Here we summarize its most relevant features and some of the new elements that are of relevance for the present work. A detailed report on the performance of these new features have also been described elsewhere [9].

Since only a simple polynomial ratio appears in the WK filter, this is implemented in the discrete time domain as 9 parameters second order A.R.M.A. algorithm applied to raw data sampled at 4882.8125 Hz.

The resulting data at the output of WK filter are very effectively band-limited (see Fig. 2) and can be subsampled in order to bury by aliasing the unmodeled features that are present outside the interesting bandwidth. Subsampling is also useful in reducing the data rate. The inverse of the matching filter $M(\omega)$ of Eq. (14) is then applied to the subsampled data, properly translated into the reduced frequency band, thus obtaining the whitened data with PSD $S_w(\omega)$.

The on-line analysis includes a built-in adaptive algorithm that updates the filter parameters to take into account their slow drift on time scales longer than an hour. For example, the core of the algorithm for the estimate of the post-filtering bandwidth [the parameters which mostly affect the signal to noise ratio (SNR)] tries to keep $S_w(\omega)$ as flat as possible. This is done for each 2 minute long buffer by comparing the values $S_w(\omega_k)$ averaged on a narrow band around the frequencies of the two modes, with that measured at a selected frequency in between. Since the difference is proportional to the error between the currently used parameters and their optimum value, it is used to drive the adaptive algorithm that adjusts the parameters.

Data in resonant detectors often contain unmodeled signals superimposed to the background Gaussian noise. When these signals dominates a stretch of data, the whitening process fails. This is recognized by the adaptive procedure that freezes in the previously adjusted value. This selection procedure allows the filter paramenters to be adjusted for drifts on a time scale longer than the mechanical relaxation time of the system, while ignoring dramatic changes due to isolated events.

When large isolated excitations are present, data are no longer gaussian especially at the high amplitude regions of the distribution. The estimate of noise parameters, in first place $\sigma_{\hat{A}}^2$, can then be affected by large biases. In order to ensure self-consistency, the analysis continuously monitors the curtosis of the data and the autocorrelation of the whitened data. If these parameters are found to be within 3 times their expected standard deviations the data buffer is accepted for the filter parameter estimate. Otherwise the filter parameters are frozen in.

If the freezing in of the parameters update occurs too frequently on contiguous data buffer, an alert flag is switched on to indicate instrument malfunctioning. Eventually these flags are the basis for the definition of vetoes on time periods of output data.

A maximum-hold algorithm is applied to the filtered data to search for candidate δ-like GW events. For each event, the time of arrival, the amplitude and χ_a^2 are estimated. The latter is derived by applying Eq. (6) to the subsampled whitened data. We use a set $\{y_i\}$ of data long about 3 times the typical

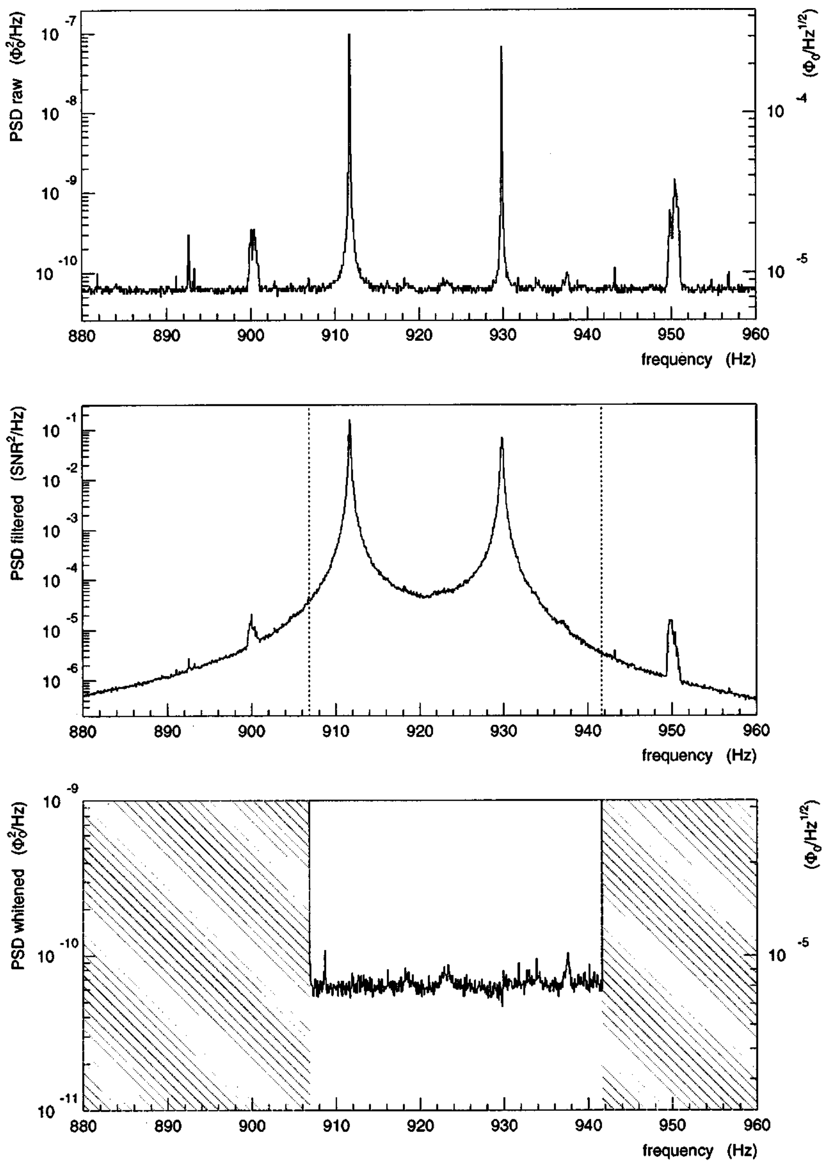

FIG. 2. The power spectral density of the raw data around the detector modes (upper) shows only small monochromatic disturbances. The PSD of the WK filtered data (middle) are effectively band-limited and therefore can be suitably subsampled keeping all the information within a 35 Hz bandwidth around the modes. In this bandwidth, the whitened data (lower) demonstrate that the parameters of the noise model were correctly estimated.

WK filter time, $2/\Delta\omega_k^{\rm opt}$, following the event arrival time. This choice ensures that the signal decays into the noise within the selected time span, for signal amplitudes up to SNR$=100$. The computed χ_a^2 is attached to the event in the event list.

VI. EXPERIMENTAL RESULTS

A sample of the whitened data taken with the cryogenic detector is shown in Fig. 2 within the reduced bandwidth. The flatness of their PSD $S_W(\omega)$ demonstrates the consistency of the model of Eq. (6) and the good matching to the parameters of the noise of the detector. The number of degrees of freedom used to compute the χ_a^2 was 211, 212 being the number of $\{y_i\}$ samples used to calculate X for this data of the cryogenic detector.

The key result of the present paper is that the estimated χ_a^2 of each candidate δ-like event does follow the reduced chi-square distribution χ_r^2, as is shown in Fig. 3 for five days of AURIGA data. In fact, at least at low SNR, the measured χ_a^2 histograms are well fitted by a chi-square distribution with the proper number of degrees of freedom, as it is expected since most of the events up to SNR$=5$ are due to statistical fluctuations of the modeled noise. In particular, the estimated amplitude $\hat{A}$ and the χ_a^2 are indeed independent random variables. The compliance with the chi-square distribution and the independence of $\hat{A}$ and χ_a^2 are a consequence of two

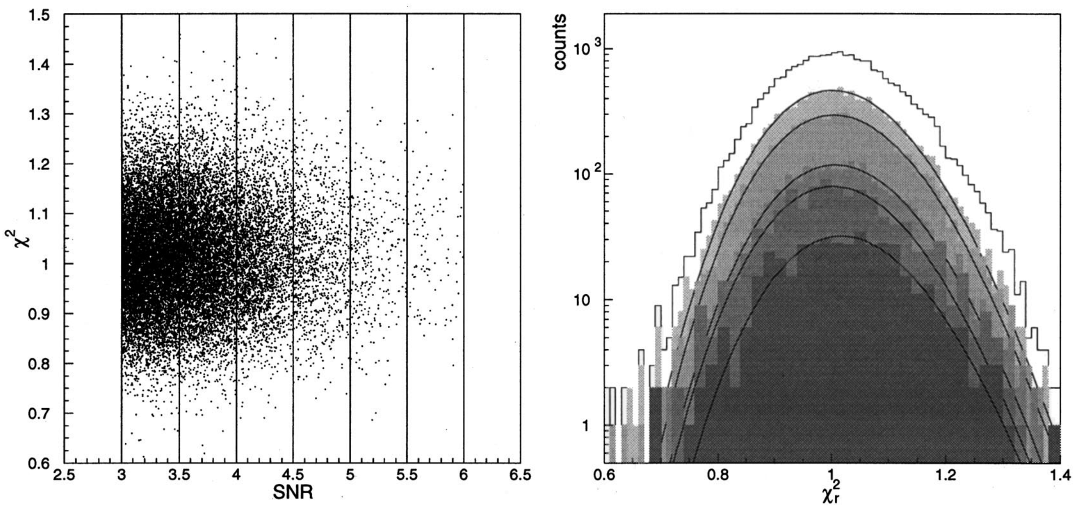

FIG. 3. Left: plot of χ_a^2 and SNR of candidate events for AURIGA with $3<\mathrm{SNR}<6$. Right: histograms of χ_a^2 of all these events (white) and of events whose SNR is between 3 and 3.5, 3.5 and 4, and so on up to between 5.5 and 6 (from brighter gray to darker gray, respectively). The continuous lines are reduced chi-square distributions χ_r^2 with 211 degrees of freedom fitted to these histograms: the agreement is evident and is independent from the SNR. The data are relative to 5 days of data taking and to about 24 000 events above SNR=3.

facts: the Gaussian nature of the detector noise as a result of the data reduction procedure described above and the consistency of low SNR events with the expected shape of a δ-like mechanical excitation of the antenna.

In order to demonstrate that the WK filter and the chi-square test would correctly recognize a δ-like gravitational wave event, a number of software calibration signals has been numerically added to the real raw data stream acquired over two days from AURIGA. These software signals were given the expected shape to which the WK filter was matched, with SNR of 30 and 45. As Fig. 4 shows, the χ_a^2 of these pulses are in reasonably good agreement with the expected reduced chi-square distribution χ_r^2 with the proper number of degrees of freedom. A slight distortion of the observed distribution is accounted for by the fluctuations of the estimate of σ_A^2.

To understand the discrimination ability of the test, we show in Fig. 5 the Fourier transform for two high SNR signals taken from the WK filtered real data, one passing the test and the other failing it. The figure shows the remarkable difference in spectral content of the two pulses. It also shows that the shape of the pulse passing the test is in very good

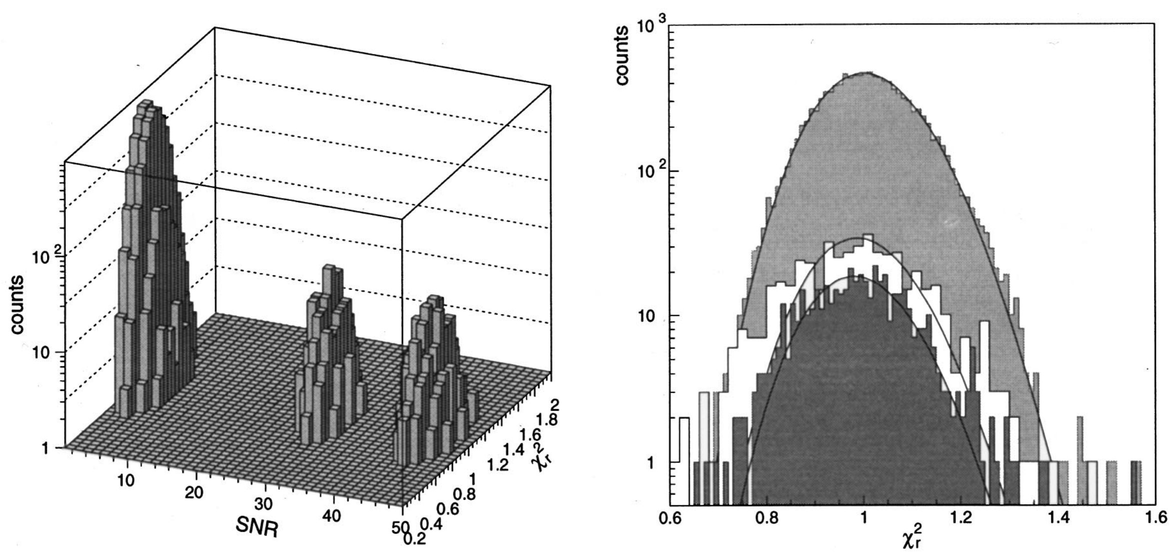

FIG. 4. Left: 3D histogram of χ_a^2 vs SNR for AURIGA. Data that cluster around SNR$\approx$30, SNR$\approx$45 and $\chi_a^2\approx1$ are due to software calibration pulses with shape matched to the WK filter which have been added on the real data stream acquired by AURIGA during 14–15 June 1997. Spurious signals are not visible in this range. Right: histograms of χ_a^2 for the low amplitude candidate events (gray area) and for the software calibration pulses (white and dark gray area).

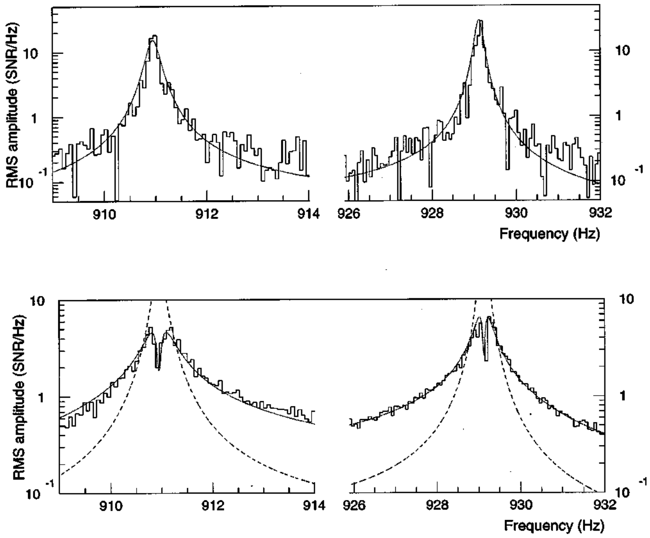

FIG. 5. Fast Fourier transform of detected candidate events pulses with SNR$=18.2$ and $\chi_a^2=1.01$ (upper) and with SNR $=23.5$ and $\chi_a^2=6.8$ (lower) at the output of the WK filter. The superimposed continuous lines represent the expected responses for a mechanical δ-like excitation of the bar (upper), and a fast electromagnetic excitation entering the ADC input or the SQUID output (lower), respectively. For comparison, the upper continuous line is also shown in the lower graph as a dashed line.

agreement with the expected one for a δ-like mechanical excitation of the bar. For the pulse failing the test, the detected pulse is in good agreement with the expected shape for an idealized electromagnetic pulse exciting the SQUID output circuit.

In Fig. 6 we show the result of the event search during the normal operation of the AURIGA detector. About 2/3 of the events with SNR>10 can be rejected because they have a $\chi_a^2>1.4$, a threshold which corresponds to a confidence level of 1.14×10^{-4} for the 211 degrees of freedom we have here. However, only a few percent of the events with SNR>5 have a χ_a^2 greater than this rejection threshold of 1.4. So, most of the events complies with the expected shape for an impulsive mechanical excitation of the resonant bar. Moreover, only about 13% of the events with SNR>5 are accounted for by the modeled noise. We are still investigating on the origin of such a large excess.

In order to assess the validity of the quadratic dependence of computed χ_a^2 on SNR in Eq. (8), we excited the room temperature resonant-bar detector with electromagnetic pulses applied at the input of the readout amplifier. In Fig. 7 we show a scatter plot of the data collected by sending a series of pulses with increasing values of SNR. The plot clearly shows the quadratic dependence of the computed χ_a^2 on SNR of signals to which the filter is mismatched. Moreover, it shows also that the standard deviation of the computed χ_a^2 is given to a first approximation by $\lambda\cdot\mathrm{SNR}^2$ times the standard deviation of the χ_r^2 distribution with the same number of degrees of freedom. This result holds for SNR high enough to make negligible the contribution of the uncertainty on SNR estimates.

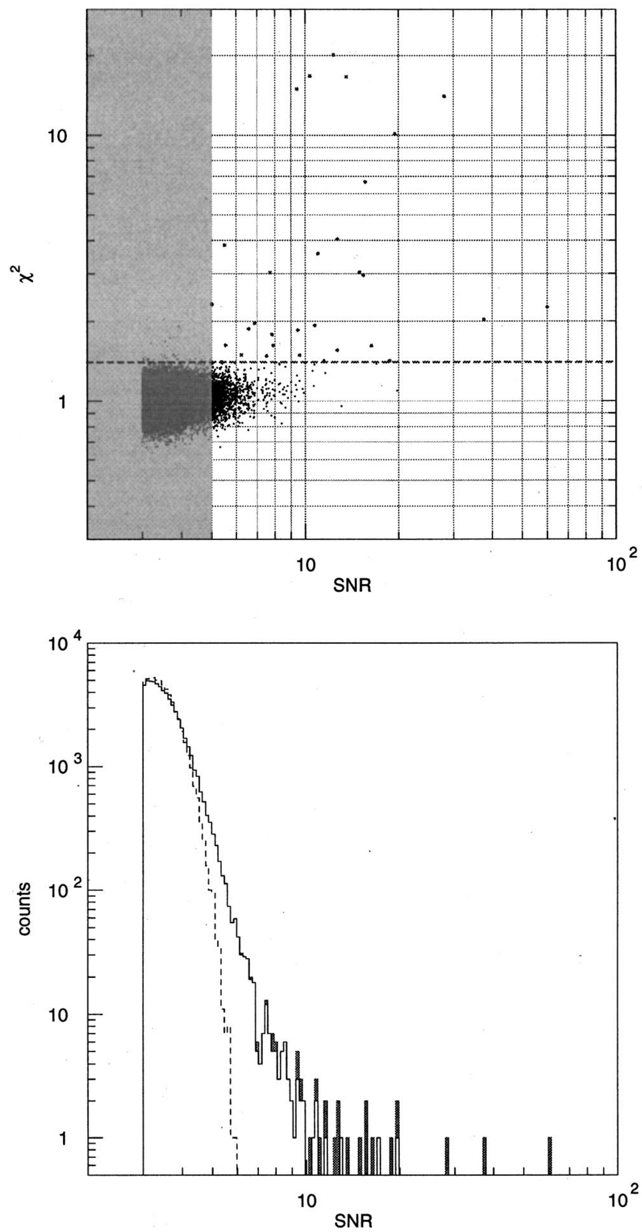

FIG. 6. Scatter plot of χ_a^2 vs SNR (upper) and SNR histogram of events with $\chi_a^2<1.4$ (white area) and for all values of χ_a^2 (white plus gray). The plots refer to 10 days of candidate events of AURIGA from 12 to 21 June 1997, corresponding to an effective observation time of 181 hours. The selected threshold of 1.4 used for the χ_r^2 test corresponds to a confidence level for false dismissal of 1.17 $\times10^{-4}$. The test allows to reduce only marginally the number of candidate events with SNR>5, from 1337 to 1306; however, for SNR>10 the χ_r^2 test vetoes about 2/3 of the events. The dashed line in the histogram is the distribution predicted with a simulated quasistationary Gaussian process, whose postdetection bandwidths follow the same time behavior of the measured ones during the observation time. It is evident that above SNR$=5$ the modeled Gaussian noise only accounts for about 13% of the detected events.

VII. DISCUSSION AND FUTURE APPLICATIONS

The reported results clearly show that at low amplitude the observed χ^2 statistics is in reasonably good agreement

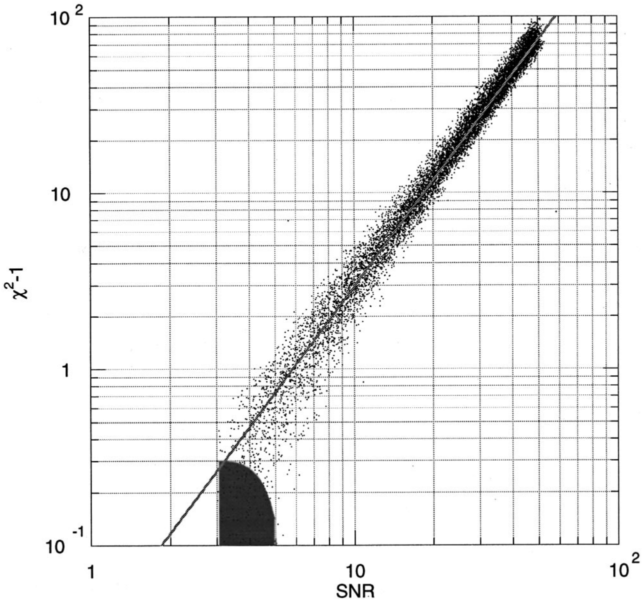

FIG. 7. Plot of computed (χ_a^2-1) vs SNR for spurious electromagnetic impulsive events, using 136 degrees of freedom. These events were generated in the room temperature detector by applying a burst excitation to the input port of the readout amplifier coupled to the motion transducer. The excitation amplitudes are uniformly distributed between SNR=0 and SNR=50. The computed χ_a^2 distribution follows a quadratic scale law, as in Eq. (8), with $\lambda=0.029$ (thick line). The gray area at low SNR stands for the low SNR background events.

with the expected one. At large amplitude the test appears to be able to discriminate between pulses with the expected signal shape and those with a different one. It is worth noticing that for pulses failing the test, a measurement of the value of the parameter λ can be used to determine the physical origin of spurious events. For instance, the type of spurious event of the AURIGA detector shown in the lower part of Fig. 5 would correspond to a $\lambda\approx0.01$; therefore theselected threshold of 1.4 on χ_r^2 would efficiently cut spurious events of this type for SNR>7 while leaving unaffected signals with proper shape to a very high confidence level.

It is worth mentioning however that the experimental χ_a^2 has a probability distribution function slightly distorted in respect to a pure χ_r^2. This is well accounted for by both the need to estimate various noise parameters from the data, a procedure that increases the spread of the distribution, and by the data being nonstationary. The confidence level can be determined empirically by using proper calibration pulses (as for the data in Fig. 4), at least for the higher false dismissal probability range.

The value of λ for electromagnetic pulses at the SQUID output of the AURIGA detector is smaller by a factor 4 than the Monte Carlo estimate $\lambda\approx0.04$ we gave in Ref. [4], but this is reasonable taking into account the different setup parameters of the detector used in the simulation. In particular the postfiltering bandwidth was ≈30 Hz for the simulation, a much higher value than the presently achieved ≈1 Hz in the detector.

Whatever the efficiency of the cleaning method described so far in rejecting spurious events, a finite amount of them survive as they are indistinguishable from gravitational wave signals. As a consequence, a single detector can only give an upper limit for the rate of GW events.

Arrays of detectors help overcome this problem. In a conventional approach, one looks for coincidences among detectors located far apart, that are assumed to be independent. Since the rate of coincidences decreases as a power law with the number of detectors in the array at the exponent, one tries to achieve conditions where the false alarm probability, as evaluated from Poisson statistics, becomes negligibly small.

The maximum likelihood–optimal filtering method, however, leads to a somewhat different procedure: one makes a global fit to the data from the N detectors in the array, of some model signal. The quantity to be minimized is then

$$\Lambda(A,t_o,\hat{n},\Psi)=\frac{1}{2}\sum_{\alpha=1}^{N}\sum_{i,k=1}^{M_\alpha}\mu_{ik}^{\alpha}\left[x^{\alpha}(t_i)-As^{\alpha}(\theta,\phi,\Psi)f\left(t_i-t_o-\frac{\vec{r}\cdot\hat{n}}{c}\right)\right]\left[x^{\alpha}(t_k)-As^{\alpha}(\theta,\phi,\Psi)f\left(t_k-t_o-\frac{\vec{r}\cdot\hat{n}}{c}\right)\right], \qquad (15)$$

where $\hat{n}$ is the wave unit vector with angles θ and ϕ, $\vec{r}$ is the position vector of the αth detector in the array with respect to a geocentric coordinate system and t_o is the signal arrival at the center of the Earth. $s^{\alpha}(\theta,\phi,\Psi)$ is a form factor that takes into account that the response of the αth detectors to the *same* incoming wave $Af(t)$ depends on its orientation in respect to the wave vector and on its polarization angle [10] Ψ.

For each choice of $\hat{n}$, t_o and Ψ, $\Lambda(A,t_o,\hat{n},\Psi)$ reaches a minimum [1] when A is the weighted average:

$$A_{\mathrm{opt}}(t_0,\hat{n},\Psi)=\frac{\sum_{\alpha=1}^{N}\frac{A_{\mathrm{opt}}^{\alpha}(t_o,\hat{n},\Psi)}{\sigma_{A\alpha}^2}}{\sum_{\alpha=1}^{N}\frac{1}{\sigma_{A\alpha}^2}}, \qquad (16)$$

where $A_{\mathrm{opt}}^{\alpha}(t_o,\hat{n},\Psi)$ is the amplitude estimate *obtained by using the data from the ath detector only*.

One can easily calculate the result that the minimum corresponding chi-square value factorizes according to

$$\chi^2(t_o,\hat{n},\Psi)\equiv 2\Lambda_{\min}(t_o,\hat{n},\Psi)=\sum_{\alpha=1}^{N}\frac{1}{\sigma_\alpha^2}\left[\sum_{i=1}^{M_\alpha} y_\alpha^2(t_i)\right]-\frac{A_{\rm opt}^2(t_o,\hat{n},\Psi)}{\sigma_A^2}$$
$$=\sum_{\alpha=1}^{N}\chi_\alpha^2(t_o,\hat{n},\Psi)+\sum_{\alpha=1}^{N}\frac{[A_{\rm opt}^\alpha(t_o,\hat{n},\Psi)-A_{\rm opt}(t_0,\hat{n},\Psi)]^2}{\sigma_{A\alpha}^2}\equiv\sum_{\alpha=1}^{N}\chi_\alpha^2(t_o,\hat{n},\Psi)+\chi_g^2(t_o,\hat{n},\Psi), \qquad (17)$$

where χ_α^2 is the chi-square one estimates by using the data from the αth detector only and χ_g^2 is the chi-square of the common weighted average $A_{\rm opt}$ of the amplitudes $A_{\rm opt}^\alpha$ estimated by each detector. It can indeed be shown that χ_g^2 is independent of all the χ_α^2's. This shows that the global chi-square test for an array of detectors can indeed be made by adding the individual chi-square values χ_α^2 for each detector to χ_g^2.

As with any multiple parameter non-linear fit, the procedure should be repeated for all $\hat{n}$ and Ψ in search for the absolute minimum. This reintroduces a correlation among the χ_α^2 and χ_g^2 as the global minimum does not coincide with the parameter values that minimize either each χ_α^2 or χ_g^2. Resonant detectors presently in operation [11] are however oriented almost parallel. In addition, full high resolution timing has been implemented up to now only for AURIGA. In practice, due to the still comparatively low bandwidth of these detectors, only phase-timing, i.e., timing modulo a period of antenna oscillation, can be done at reasonable signal-to-noise ratio [8]. As a consequence, each detector produces a list of candidate events with a time of arrival only known within a fraction of a second. Coincidence analysis [12] is then performed with a time window of the same order.

Within this somehow coarse procedure Eq. (17) still indicates that χ_g^2 can be used as a reference statistics to tests for the consistency of amplitude of a candidate coincidence event. With 5 detectors χ_g^2 is distributed chi-square with 4 degrees of freedom. Application of this test to data from the IGEC [12] detectors is currently under study.

ACKNOWLEDGMENTS

We wish to acknowledge the precious work of the colleagues who helped us in setting up the AURIGA detector, in particular M. Biasotto, E. Cavallini, D. Carlesso, S. Caruso, R. Macchietto, and S. Paoli. We are also indebted for helpful discussions with G. V. Pallottino and I. S. Heng. This work has been supported in part by a grant from M.U.R.S.T.-COFIN.

[1] S. Vitale *et al.*, Nucl. Phys. **B48**, 104 (1996).
[2] G. A. Prodi *et al.*, in *Gravitational Waves: Proceedings of the Second Edoardo Amaldi Conference*, CERN, Geneva, 1997, edited by E. Coccia, G. Veneziano, and G. Pizzella (World Scientific, Singapore, 1998), pp. 148–158.
[3] C. W. Helstrom, *Statistical Theory of Signal Detection* (Pergamon, Oxford, 1968).
[4] S. Vitale, G. A. Prodi, J. P. Zendri, A. Ortolan, L. Taffarello, G. Vedovato, M. Cerdonio, and D. Pascoli, in *Gravitational Waves, Sources and Detectors*, Proceedings of the International Conference, edited by F. Fidecaro and I. Ciufolini (World Scientific, Singapore, 1997), p. 256.
[5] See, e.g., J. C. Price, Phys. Rev. D **36**, 3555 (1987); M. Cerdonio *et al.*, Physica B **194–196**, 3 (1994).
[6] A. Ortolan, G. Vedovato, M. Cerdonio, and S. Vitale, Phys. Rev. D **50**, 4737 (1994).
[7] A. Ortolan *et al.*, in *Gravitational Waves: Proceedings of the Second Edoardo Amaldi Conference*, CERN, Geneva, 1997, edited by E. Coccia, G. Veneziano, and G. Pizzella (Ref. [2]), pp. 204–215.
[8] V. Crivelli-Visconti *et al.*, Phys. Rev. D **57**, 2045 (1998).
[9] L. Baggio *et al.*, *Proceedings of the Third Edoardo Amaldi Conference*, Caltech, Pasadena, CA, 1999 (in press); G. A. Prodi *et al.*, *ibid.*
[10] Here a purely polarized wave is assumed in order not to make the algebra too heavy. Extension to arbitrary polarization is straightforward.
[11] ALLEGRO at University of Louisiana, Baton Rouge, USA, AURIGA at INFN Natl. Lab. of Legnaro, Italy, EXPLORER at CERN, Switzerland, NAUTILUS at INFN Natl. Lab. of Frascati, Italy, and NIOBE at University of Western Australia, Perth, Australia.
[12] Within the International Gravitational Event Collaboration, IGEC.

First Search for Gravitational Wave Bursts with a Network of Detectors

Z. A. Allen,[1] P. Astone,[2] L. Baggio,[3] D. Busby,[1] M. Bassan,[4,5] D. G. Blair,[6] M. Bonaldi,[7] P. Bonifazi,[8,2] P. Carelli,[9] M. Cerdonio,[3] E. Coccia,[4,5] L. Conti,[3] C. Cosmelli,[10,2] V. Crivelli Visconti,[3] S. D'Antonio,[11] V. Fafone,[11] P. Falferi,[7] P. Fortini,[12] S. Frasca,[10,2] W. O. Hamilton,[1] I. S. Heng,[1] E. N. Ivanov,[6] W. W. Johnson,[1] M. Kingham,[1] C. R. Locke,[6] A. Marini,[11] V. Martinucci,[13] E. Mauceli,[11] M. P. McHugh,[1] R. Mezzena,[13] Y. Minenkov,[5] I. Modena,[4,5] G. Modestino,[11] A. Moleti,[4,5] A. Ortolan,[14] G. V. Pallottino,[10,2] G. Pizzella,[4,11] G. A. Prodi,[13,*] E. Rocco,[3] F. Ronga,[11] F. Salemi,[10] G. Santostasi,[1] L. Taffarello,[15] R. Terenzi,[8,5] M. E. Tobar,[6] G. Vedovato,[13] A. Vinante,[13] M. Visco,[8,5] S. Vitale,[13] L. Votano,[11] and J. P. Zendri[15]

(International Gravitational Event Collaboration)

[1]*Department of Physics and Astronomy, Louisiana State University, Baton Rouge, Louisiana 70803*
[2]*I.N.F.N., Sezione di Roma1, Piazzale Aldo Moro 2, I-00185, Roma, Italy*
[3]*Dipartimento di Fisica, Università di Padova, and I.N.F.N., Sezione di Padova, Via Marzolo 8, 35131 Padova, Italy*
[4]*Dipartimento di Fisica, Università di Roma "Tor Vergata," Via Ricerca Scientifica 1, I-00133 Roma, Italy*
[5]*I.N.F.N., Sezione di Roma2, Via Ricerca Scientifica 1, I-00133 Roma, Italy*
[6]*Department of Physics, University of Western Australia, Nedlands, WA 6907 Australia*
[7]*Centro di Fisica degli Stati Aggregati, I.T.C.-C.N.R., and I.N.F.N., Gruppo Collegato di Trento, I-38050 Povo, Trento, Italy*
[8]*Istituto Fisica Spazio Interplanetario, C.N.R., Via Fosso del Cavaliere, I-00133 Roma, Italy*
[9]*Dipartimento di Fisica, Università de L'Aquila, and I.N.F.N., L'Aquila, Italy*
[10]*Dipartimento di Fisica, Università di Roma "La Sapienza," Piazzale Aldo Moro 2, I-00185, Roma, Italy*
[11]*I.N.F.N., Laboratori Nazionali di Frascati, Via E. Fermi 40, I-00044, Frascati, Italy*
[12]*Dipartimento di Fisica, Università di Ferrara, and I.N.F.N., Sezione di Ferrara, I-44100 Ferrara, Italy*
[13]*Dipartimento di Fisica, Università di Trento, and I.N.F.N., Gruppo Collegato di Trento, I-38050 Povo, Trento, Italy*
[14]*Laboratori Nazionali di Legnaro, Istituto Nazionale di Fisica Nucleare, 35020 Legnaro, Padova, Italy*
[15]*I.N.F.N., Sezione di Padova, Via Marzolo 8, I-35131 Padova, Italy*

(Received 19 June 2000)

We report the initial results from a search for bursts of gravitational radiation by a network of five cryogenic resonant detectors during 1997 and 1998. This is the first significant search with more than two detectors observing simultaneously. No gravitational wave burst was detected. The false alarm rate was lower than 1 per 10^4 yr when three or more detectors were operating simultaneously. The typical threshold was $H \simeq 4 \times 10^{-21}$ Hz^{-1} on the Fourier component at $\sim 10^3$ Hz of the gravitational wave strain amplitude. New upper limits for amplitude and rate of gravitational wave bursts have been set.

PACS numbers: 95.85.Sz, 04.80.Nn

The direct detection of gravitational waves will be a watershed event for both the physics of gravitation and the investigation of compact astronomical objects. A variety of astrophysical events is expected to produce gravitational waves of short duration ($\ll$1 s), or *gw bursts,* such as the gravitational collapse of stars or the final few orbits and the subsequent coalescence of a close binary system of neutron stars (NS's) or black holes (BH's) [1]. Because of the inherent weakness of such signals, and the difficulty in distinguishing them from a myriad of noise sources, the direct detection of a gw burst will require coincident detection by multiple detectors with uncorrelated noise. Searches for gw bursts over periods of observation of 1–3 months have been performed in the past by pairs of cryogenic resonant bar detectors [2–4], setting upper limits on the incoming rate. A few days of observation have been reported for simultaneous operation of three cryogenic bar detectors [2] and, with much less sensitivity, of a pair of short-arm interferometric detectors [5]. Upper limits on gw signals from coalescing binaries have been recently reported also by a single interferometric detector for 25 hours of observation [6].

In the last few years, the increase of the number of cryogenic resonant detectors in simultaneous operation has greatly improved the prospects of obtaining a confident detection of gw bursts. There are now five operational cryogenic bar detectors: ALLEGRO (Baton Rouge, Louisiana, U.S.A.) [7], AURIGA (Legnaro, Italy) [8], EXPLORER (CERN) [9], NAUTILUS (Frascati, Italy) [10], and NIOBE (Perth, Australia) [11]. The groups operating these detectors agreed in 1997 to start a global search for short ($\sim$1 ms) gw bursts under common protocols, by establishing the International Gravitational Event Collaboration (IGEC) [12].

All these detectors use the same principles of operation. The gw excites the first longitudinal mode of the cylindrical bar, which is cooled to cryogenic temperatures to reduce the thermal noise and is isolated from seismic and acoustic disturbances. To measure the strain of the bar, a secondary mechanical resonator tuned to the cited mode is mounted on one bar face and a sensor measures the displacement between the secondary resonator and the bar face. The resulting noise of the detectors in terms of strain at the input is (5–10) $\times 10^{-22}$ Hz$^{-1/2}$ in a bandwidth of $\sim$1 Hz

 0031-9007/00/85(24)/5046(5)$15.00

TABLE I. Main characteristics of the IGEC cryogenic bar detectors. The detectors measure the mean Fourier component H of the gw in the detection bandwidth of $\sim$1 Hz around the mode frequencies. $H = (4L\nu^2)^{-1}\sqrt{E/M}$, where E is the energy deposited in the bar by the gw and ν is the mean of the mode frequencies. The bars are made by Al5056 except for NIOBE, whose bar is made of Nb. The sub-kelvin detectors and NIOBE showed very similar typical energy sensitivity in 1997–1998, better by a factor of about 4 with respect to the other detectors. The differences in mass and material, though, affect the gw sensitivity and give a conversion factor from $\sqrt{E}$ to H which is 2.3 times worse for NIOBE than for the other detectors.

Detector	ALLEGRO	AURIGA	EXPLORER	NAUTILUS	NIOBE
Mode frequencies (Hz)	895, 920	912, 930	905, 921	908, 924	694, 713
Bar mass M (kg)	2296	2230	2270	2260	1500
Bar length L (m)	3.0	2.9	3.0	3.0	2.75
Bar temperature (K)	4.2	0.2	2.6	0.1	5.0
Longitude	$91°10'44''W$	$11°56'54''E$	$6°12'E$	$12°40'21''E$	$115°49'E$
Latitude	$30°27'45''N$	$45°21'12''N$	$46°27'N$	$41°49'26''N$	$31°56'S$
Azimuth	$40°W$	$44°E$	$39°E$	$44°E$	$0°$

surrounding the two coupled-mode frequencies. Some of the important physical parameters of the five detectors are shown in Table I. The detector response is optimal for a gw incoming perpendicular to the bar axis and polarized along it [13]. The axes of all the bar detectors are aligned to within a few degrees of one another, so that the chance of coincidence detection is maximized. This makes the amplitude acceptance of the detectors for the Galactic center direction greater than 0.7 for about 60% of the time [14].

Each detector output is processed by filters optimized for short gw bursts, giving the estimate for the Fourier component $H(\omega)$ of the strain amplitude $h(t)$ in the detection bandwidth of $\sim$1 Hz around the mode frequencies listed in Table I. More specifically, $h(t)$ is the gw amplitude multiplied by the antenna pattern of the detector [13]. With the exception of the ALLEGRO detector, the noise of the detectors was typically not stationary over long observation times and was affected by some unmodeled noise sources, whose correlation with common environmental noise sources was found to be weak [15]. Figure 1 shows the variability of the noise of each detector during 1997–1998, in terms of the Fourier component of the

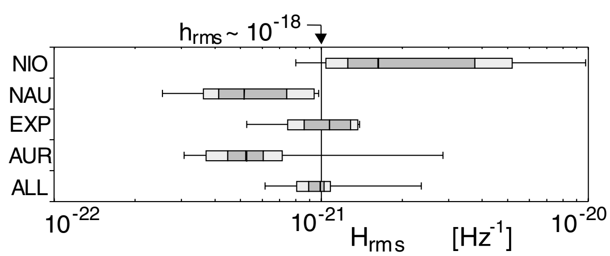

FIG. 1. Spread of the noise of detectors during 1997–1998 in terms of the Fourier component H_{rms} of the gw at SNR = 1. The plotted bands of variability of the noise are delimited by selected percentiles, i.e., by selected fractions of the observation time for which the sensitivity has been better than H_{rms}: innermost tick 50%, gray band 16%–84%, white band 2.5%–97.5%, and "T" lines 0%–100%. The corresponding gw amplitude h_{rms} for a $\sim 10^{-3}$ s burst is sketched in the upper scale.

gw corresponding to unity signal-to-noise ratio, H_{rms}. The detectors had quite similar noise levels, since the typical values of H_{rms} were all within a factor of 3.

We point out that this search for bursts is suitable for any transient gw which shows a nearly flat Fourier transform $H(\omega)$ of its amplitude $h(t)$ at the two resonant frequencies of each detector. The metric perturbation $h(t)$ can either be a millisecond pulse, a signal made by a few millisecond cycles, or a signal sweeping in frequency through the detector resonances. The IGEC search is therefore sensitive to different kinds of gw sources such as a stellar gravitational collapse [1], the last stable orbits of an inspiraling NS or BH binary, its merging, and its final ringdown [16]. The computation of h from the measured Fourier component H requires a model for the signal shape. A conventionally chosen shape is a pulse lasting $\sim 10^{-3}$ s [17]; in this case, H should be multiplied by $\sim 10^3$ Hz to get the corresponding strain amplitude, h.

This Letter reports the results of the first coincidence search for gw bursts performed by the IGEC observatory. The observations covered most of 1997–1998, including 625.0 days with at least one detector in operation, 260.4 days with at least two detectors in simultaneous operation, 89.7 days with three detectors, and 15.5 days with four. This is the first search with significant observation time with more than two detectors. The duration of simultaneous operation would have been greater if it had been possible to operate these instruments with higher duty factors, which were typically $\lesssim$50% during this period with the exception of ALLEGRO. More details on the observatory, its data exchange protocol, and the exchanged data set can be found in Ref. [14].

The analysis of the data can be divided into two parts: a generation of candidate *event lists* for each of the individual detectors, and a time coincidence analysis using the lists. This approach, though not optimal, has the advantage of being easily implemented and provides for a satisfactory effectiveness.

Each IGEC group extracted the candidates for gw bursts, or *events,* by applying a threshold to the filtered output of the detector. The events were described by their Fourier magnitude H, their arrival time, the detector noise at that time, and other auxiliary information. To limit the expected rate of accidental coincidences, each detector threshold was adaptively set to obtain a maximum event rate of $\sim$100 per day, with typical values in the range $H_{\mathrm{det}} \sim (2-6) \times 10^{-21}\ \mathrm{Hz}^{-1}$ corresponding to magnitude signal-to-noise ratio SNR $\simeq 3-5$. Single spurious excitations are vetoed against disturbances detected by environmental sensors. The AURIGA detector checked each event against the expected waveform template by means of a χ^2 test [18]. The lists of the events exchanged within IGEC by each detector also include declarations of the off and on times for the detectors.

All searches for coincident events used a time window of 1.0 s. This choice limits the false dismissal probability to less than a few per cent while it ensures a very low false alarm probability when at least three detectors are observing simultaneously. No three- and fourfold coincidence was detected, and therefore we did not identify candidates for gravitational wave detection in the 89.7 days of threefold observation. The detector thresholds were typically $3 \times 10^{-21}\ \mathrm{Hz}^{-1}$ for the most sensitive threefold configuration (ALLEGRO-AURIGA-NAUTILUS) and $5 \times 10^{-21}\ \mathrm{Hz}^{-1}$ for the others. To give examples of detectable signals, these thresholds would correspond to, respectively, $\sim 0.04 M_{\odot}$ and $0.11 M_{\odot}$ converted to isotropic radiation in the optimal polarization at the distance of the Galactic center (10 kPc), assuming a gw burst of 1 ms duration [17]. For comparison, the signal expected from the last stable orbits of an optimally oriented NS coalescing binary at 10 kPc with $2 \times 1.4 M_{\odot}$, would give $H(\omega) = (3-4) \times 10^{-21}\ \mathrm{Hz}^{-1}$ at the detector resonant frequencies. The number and amplitude of the twofold coincidences found in the 260.4 days of twofold observation are in agreement with the estimated accidental background [14].

The estimation of the false alarm rate is a crucial element in any gw search. It allows for the interpretation of any observed coincidences as well as the evaluation of the potential of the observatory. Since the events arrival times of each detector are randomly distributed with a nonstationary rate, the expected background of accidental coincidences can be computed by two methods: (i) by modeling the event times as Poisson point process and using the measured rates of events for each detector, and (ii) by counting the coincidences after performing even time shifts of the event times of one detector with respect to the others [2].

In the first approach, the expected rate of accidental coincidences is [19]

$$\lambda = N \frac{(\Delta t)^{N-1}}{T_{\mathrm{obs}}^{N}} \prod_{i=1}^{N} n_i \,, \qquad (1)$$

where N is the number of detectors simultaneously operating, T_{obs} their common observation time, $\Delta t = 1$ s the maximum time separation for a coincidence, and n_i the number of events of the ith detector during T_{obs}. This equation holds even if the event rates of detectors are not stationary as long as they are uncorrelated among different detectors.

The second approach is more empirical. In the case of the twofold coincidence searches, the time shift results are in agreement with those predicted through Eq. (1) [14], and demonstrate that the event rates of different detectors are uncorrelated.

The capabilities of the IGEC observatory with respect to the false alarm probability are shown in Fig. 2 for a few sample configurations of the observatory. The accidental rate is calculated as a function of a signal amplitude threshold H_{thr} at the detectors by applying Eq. (1) to the number of events of the detectors whose amplitude is $\geq H_{\mathrm{thr}}$. The typical time variability of the instantaneous accidental rate λ has been calculated by means of a Monte Carlo simulation based on the measured nonstationary behavior of event rates on single detectors. This variability is about 1 order of magnitude with respect to the mean and is mainly determined by the nonstationary performances of the detectors. The estimated mean background of twofold coincidences is still fairly high, unless H_{thr} is raised well above the data exchange threshold H_{det}. On the other

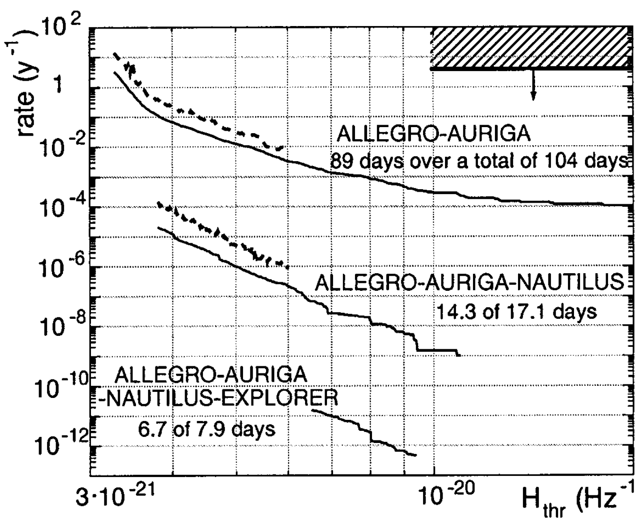

FIG. 2. Estimated rate of accidental coincidences, $\lambda(\mathrm{yr}^{-1})$, versus the threshold $H_{\mathrm{thr}}(\mathrm{Hz}^{-1})$ for a sample pair, triple, and four-tuple of detectors in 1997–1998. The continuous lines show the mean value of λ for signal amplitudes $\geq H_{\mathrm{thr}}$. The dashed lines represent the 1 standard deviation upper bounds for the time variation of the instantaneous accidental rates. This figure takes into account the best 85% of common observation times, when every detector had an event search threshold lower than 3.25, 3.8, and $6.5 \times 10^{-21}\ \mathrm{Hz}^{-1}$, respectively, for the pair, the triple, and the four-tuple. The λ's for the other operative configurations of detectors were similar, allowing for a small increase of the corresponding H_{thr}, at most by a factor of 2. The bold horizontal line with arrow stands for the new upper limit set by all IGEC detectors on the rate of incoming gw bursts during 1997–1998.

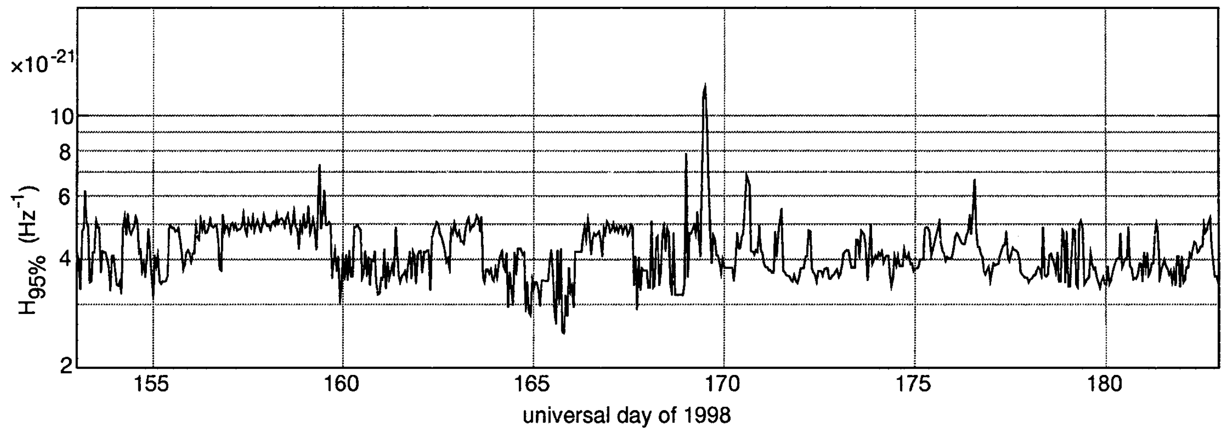

FIG. 3. A sample of the upper limit with 95% confidence on the amplitude of single gw bursts incident with optimal polarization and orientation on the IGEC observatory hour by hour in June 1998. The highest peaks shown are due to single high amplitude events of one detector while the others were not operating.

hand, a threefold or fourfold coincidence search keeps a high statistical significance even for $H_{\rm thr} \sim H_{\rm det}$, since the expected accidental rates are low enough: respectively, less than one false alarm per 10^4 or 10^6 yr of observation at $H_{\rm thr} \sim 4 \times 10^{-21}$ Hz^{-1}. These fall rapidly as $H_{\rm thr}$ increases. In fact, the IGEC accidental background noise would remain negligible even after centuries of observation time.

The 260 days of observation with two or more detectors in simultaneous operation improved by about a factor of 3 the previously set upper limit on the rate of gw bursts incident on the Earth [3]. Assuming the emission is described by a stationary Poisson point process and using the same procedure as in Refs. [2,3], the limiting rate set for a gw burst emission from isotropically distributed sources is $\leq$4 yr^{-1} for $H_{\rm gw} \geq 10^{-20}$ Hz^{-1} (Fig. 2) with 95% confidence. A more complete analysis is in progress.

The IGEC observatory can also be used to set an upper limit on the amplitude of gw bursts corresponding to astronomical events, such as supernovae or gamma ray bursts. For time windows of the order of the hour or larger, each detector is likely to show accidental events and therefore this upper limit benefits from a multiple coincidence search among the operating detectors.

A sample of the upper limits on the amplitude of gw bursts occurring within a time span of 1 h, is shown in Fig. 3 for a few weeks of 1998, when up to four detectors were operating. These limits apply to the component of the radiation emitted with optimal polarization from a source optimally oriented with respect to the detectors. We are 95% confident that there was no radiation above this level hour by hour. In all of 1998, the limits set by the IGEC observatory were better than $H_{\rm gw} = 6$ and 4×10^{-21} Hz^{-1} for 94% and 21% of the year, respectively. To specialize these upper limits for a specific source direction, each detector response should be divided by its antenna pattern [13]. The corresponding observation times of the Galactic center by IGEC within the same limits have been, respectively, 44% and 7.5% of 1998. For a source at the Galactic center emitting isotropically a 1 ms burst [17], the above upper limits correspond to about $0.16 M_\odot$ and $0.07 M_\odot$ converted in the optimal polarization.

Finally, we remark that the IGEC observatory is capable of monitoring the strongest galactic sources with a very low false alarm probability when at least three detectors are simultaneously operating. All the groups involved are actively working for upgrading the current detector performances and therefore we expect in the near future to extend the observation range to the Local Group of galaxies, which means an increase of a factor of 10 of the observed mass.

The ALLEGRO group was supported by the National Science Foundation Grant No. 9970742 and LSU, the NIOBE group by the Australian Research Council, and the Italian groups by the Istituto Nazionale di Fisica Nucleare and in part by a grant COFIN'97 from Ministero dell'Universitá e della Ricerca Scientifica e Tecnologica.

*Corresponding author.
Email address: prodi@science.unitn.it

[1] See, for instance, B. F. Schutz, Classical Quantum Gravity **16**, A131 (1999).
[2] E. Amaldi *et al.,* Astron. Astrophys. **216**, 325 (1989).
[3] P. Astone *et al.,* Phys. Rev. D **59**, 122001 (1999).
[4] P. Astone *et al.,* Astropart. Phys. **10**, 83 (1999).
[5] D. Nicholson *et al.,* Phys. Lett. A **218**, 175 (1996).
[6] B. Allen *et al.,* Phys. Rev. Lett. **83**, 1498 (1999).
[7] E. Mauceli *et al.,* Phys. Rev. D **54**, 1264 (1997).
[8] G. A. Prodi *et al.,* in *Proceedings of the Second Edoardo Amaldi Conference,* edited by E. Coccia *et al.* (World Scientific, Singapore, 1998), pp. 148–158.
[9] P. Astone *et al.,* Phys. Rev. D **47**, 362 (1993); from 1998 Explorer is a CERN Recognized Experiment.
[10] P. Astone *et al.,* Astropart. Phys. **7**, 231 (1997).

[11] D. G. Blair *et al.,* Phys. Rev. Lett. **74**, 1908 (1995).
[12] See http://igec.lnl.infn.it
[13] A bar detector detects the fraction $\sin^2(\theta)\cos(2\psi)$ of the amplitude of an incident gw, where θ is the angle between the bar axis and the gw direction and ψ is the polarization angle of the gw in the wave front plane with respect to the bar axis.
[14] G. A. Prodi *et al.,* Int. J. Mod. Phys. D **9**, 237 (2000).
[15] I. S. Heng *et al.,* Phys. Lett. A **218**, 190 (1995).
[16] E. E. Flanagan and S. A. Hughes, Phys. Rev. D **57**, 4535 (1998).
[17] See, for instance, M. Cerdonio *et al.,* in *Proceedings of the GR15 Conference,* edited by N. Dadhich and J. Narlikar (IUCAA, India, 1998), p. 211.
[18] L. Baggio *et al.,* Phys. Rev. D **61**, 102011 (2000).
[19] See, for instance, R. K. Bock *et al., Data Analysis Techniques for High-Energy Physics Experiments* (Cambridge University, Cambridge, England, 1990), p. 22; for nonstationary Poisson point processes: A. Papoulis, *Probability, Random Variables and Stochastic Processes* (McGraw-Hill, New York, 1984).

Conclusions

AURIGA data analysis is capable of optimal gw burst characterization. A combination of hardware and software characteristics let it have a very small timing error, which – with other 3 detectors of equal sensitivity – either would allow to spot in the sky the exact direction of the incoming wave, or to reject the signal as spurious, through a maximum likelihood method.

Even without timing capability, an observatory implementing goodness-of-the-fit tests on the event waveform would reject most of the spurious signals at high SNR. With respect to other methods implementing an equivalent 1 degree of freedom test, the χ^2 test of 3 or 4 detector would allow from a hundred to a thousand degrees of freedom, letting therefore just a small window of possibilities for an accidental coincidence to be accepted.

However, amplitude estimates, time of arrivals and χ^2 calculations are all still computed with the picture of a stationary-modeled noise. Unless new hardware improvements calms down the detector non-stationary behavior, the analysis will suffer a big loss in duty cycle, due to the necessity to identify good operational periods in the most robust way, to keep low the probability of a false dismissal. This in turn has serious consequences on the IGEC observatory performances, as there is little chance to have more than few weeks of common 4-fold operation between detectors if the duty cycle stays below 50% on the single detector.

One of the most impelling tasks is therefore to push on new methods of filter adaptiveness and data validation.

Fast noise transients and filter parameter misestimate both could introduce biases. Investigation with Monte Carlo techniques now available can provide in the future some on-line hint to trigger a recalibration of the filter parameters or to set finer (and maybe amplitude-dependent) automatic veto.

The performance of the filter algorithm could be improved with also with a radical change of the filter, for example abandoning the Wiener-Kolmogorv static filter for a real adaptive Kalman filter approach [38].

As for future of IGEC, we should as soon as possible try to exchange pre-event search data, and in the form of a common data format, and methods for correlation analysis should be developed.

Convention, notations and symbols

$x, y, t, z, n, i, j, \ldots$	real, complex or integer scalars
$\mathbf{x}, \mathbf{y}, \mathbf{M}, \mathbf{N}, \ldots$	vectors or arrays
$\mathtt{n}, \mathtt{t}, \mathtt{i}, \ldots$	stochastic process
ν , $\omega = 2\pi\nu$	frequency in Hz and in rad/s
$x * y(t) \equiv x(t) * y(t) \equiv \int_{-\infty}^{+\infty} x(t-\tau) y(\tau) d\tau$ continuous case $\equiv \sum_{-\infty}^{+\infty}{}_j x_{i-j} y_j$ discrete case	signal convolution
$T \circ \mathrm{f}(t) \equiv \int_{-\infty}^{+\infty} \mathrm{t}(\tau)\, \mathrm{f}(t-\tau) dt \quad \Leftrightarrow \quad T \circ \tilde{\mathrm{f}}(\omega) \equiv \mathrm{T}(\omega)\, \tilde{\mathrm{f}}(\omega)$	effect of the linear system T on the signal f
$\tilde{\mathrm{f}}(\omega) \equiv \int_{-\infty}^{+\infty} \mathrm{f}(t) e^{i\omega t} dt \quad \Leftrightarrow \quad \mathrm{f}(\omega) = \frac{1}{2\pi} \int_{-\infty}^{+\infty} \tilde{\mathrm{f}}(t) e^{-i\omega t} d\omega$	Fourier transform, direct and inverse
$E\{x\}$	mean of RV x
$\sigma_x^2 \equiv \mathrm{Var}(x) = E\left\{ \left(x - E\{x\} \right)^2 \right\}$	variance of RV x
$\mathrm{erf}(x) \equiv \frac{1}{\sqrt{2\pi}} \int_{-x}^{+x} e^{-\frac{x}{2}} dx$	error function

ADC	analog to digital converter
ARMA	autoregressive moving average
CL	confidence level
daq	data acquisition
FT	Fourier transform
gw	gravitational wave
MLM	maximum likelihood method
pdf	probability density function
PSD	power spectral density
SNR	signal-to-noise-ratio
SQUID	superconducting quantum device
ToA	time of arrival
WK	Wiener-Kolmogorov
T / ω_0	carrier period/frequency
T_* / ω_*	beating period/frequency
Δt_ϕ	superconducting quantum device
t_w	coincidence time window
t_W	Wiener time

Useful results

MODEL OF THE TRANSFER FUNCTION OF A DOUBLE NORMAL MODE SYSTEM:

Transfer function:

$$\tilde{u}_\delta(\omega) = \alpha \prod_{k=1}^{2} \frac{i\omega}{\left(i\omega - p_k\right)\left(i\omega - p_k^*\right)} \qquad p_k = \omega_k\left(i + \varepsilon_k\right)$$

Impulse response:

$$u_\delta(t) = \frac{\alpha}{A(\omega_0,\omega_1,\varepsilon_0,\varepsilon_1)} \times$$

$$\times \begin{Bmatrix} e^{\varepsilon_0\omega_0 t}\left[B(\omega_0,\omega_1,\varepsilon_0,\varepsilon_1)\cos(\omega_0 t) + C(\omega_0,\omega_1,\varepsilon_0,\varepsilon_1)\sin(\omega_0 t)\right] + \\ + e^{\varepsilon_1\omega_1 t}\left[B(\omega_1,\omega_0,\varepsilon_1,\varepsilon_0)\cos(\omega_1 t) + C(\omega_1,\omega_0,\varepsilon_1,\varepsilon_0)\sin(\omega_1 t)\right] \end{Bmatrix}$$

where

$$A(\omega_0,\omega_1,\varepsilon_0,\varepsilon_1) \equiv \left[\omega_0^2\left(1+\varepsilon_0^2\right) + \omega_1^2\left(1+\varepsilon_1^2\right)\right]^2 - 4\omega_0\omega_1\left[\varepsilon_0\varepsilon_1\omega_0^2\left(1+\varepsilon_0^2\right) + \varepsilon_0\varepsilon_1\omega_1^2\left(1+\varepsilon_1^2\right) + \omega_0\omega_1\left(1-\varepsilon_0^2\varepsilon_1^2\right)\right]$$

$$B(\omega_0,\omega_1,\varepsilon_0,\varepsilon_1) \equiv \omega_0\omega_1\left[\varepsilon_0\omega_1\left(1+\varepsilon_1^2\right) - \varepsilon_1\omega_0\left(1+\varepsilon_0^2\right)\right]$$

$$C(\omega_0,\omega_1,\varepsilon_0,\varepsilon_1) \equiv \left[\omega_0^3\left(1+2\varepsilon_0^2\right) - \omega_0\omega_1^2(1+\varepsilon_1^2)\left(1+\varepsilon_0^2\right) - 2\varepsilon_0\varepsilon_1\omega_0^2\omega_1\left(1+\varepsilon_0^2\right)\right]$$

$$u_\delta(t) \xrightarrow{\varepsilon_0\approx\varepsilon_1\approx 0} \frac{\alpha}{\left(\omega_0^2-\omega_1^2\right)}\left[\omega_0 e^{\varepsilon_0\omega_0 t}\sin(\omega_0 t) - \omega_1 e^{\varepsilon_1\omega_1 t}\sin(\omega_1 t)\right]$$

WK FILTER FOR IMPULSIVE FORCE:

Transfer function

$$W(\omega) = \sigma_{\mathbf{a}}^2 S_0^{-1} \prod_{k=1}^{2} \frac{-i\omega\left(i\omega - p_k\right)\left(i\omega - p_k^*\right)}{\left(i\omega - q_k\right)\left(i\omega + q_k\right)\left(i\omega - q_k^*\right)\left(i\omega + q_k^*\right)}.$$

WHITENING FILTER:

$$L(\omega) = S_0^{-1/2} \prod_{k=1}^{2} \frac{\left(i\omega - p_k\right)\left(i\omega - p_k^*\right)}{\left(i\omega - q_k\right)\left(i\omega - q_k^*\right)}$$

GW SIGNAL TEMPLATE AFTER THE WK FILTER:

Frequency domain

$$W \circ \tilde{u}_\delta(\omega) = A\sigma_{\mathbf{a}}^2 S_0^{-1} \prod_{k=1}^{2} \frac{\omega^2}{\left(i\omega - q_k\right)\left(i\omega + q_k\right)\left(i\omega - q_k^*\right)\left(i\omega + q_k^*\right)} \qquad q_k = \omega_k\left(i + \mathrm{E}_k\right)$$

Time domain

$$W \circ u_\delta(t) = \frac{1}{D(\omega_1,\omega_2,E_1,E_2)} \sum_{k=1}^{2} \omega_k e^{-\left|tE_k\omega_k\right|}\left[\frac{1}{\left|E_k\right|}E(\omega_1,\omega_2,E_1,E_2)\cos(\omega_k t - t_0) + F(\omega_1,\omega_2,E_1,E_2)\sin(\omega_k t - t_0)\right]$$

$$\xrightarrow{E_0\approx 0; E_1\approx 0;} \frac{\alpha}{64\omega_*^2\omega_0^2} \sum_{k=1}^{2} \tau_k \omega_k^2 e^{-\frac{|t|}{\tau_k}}\left[\cos(\omega_k t - t_0) + \frac{1}{\tau_k\omega_k}\left(1 - \frac{\omega_k^4}{4\omega_*^2\omega_0^2}\right)\sin(\omega_k t - t_0)\right];$$

where

$$\omega_0 \equiv \frac{\omega_1 + \omega_2}{2}; \quad \omega_* \equiv \frac{\omega_2 - \omega_1}{2}; \quad \tau_k \equiv \frac{1}{E_k \omega_k}$$

$$D(\omega_1, \omega_2, E_1, E_2) \equiv 4 \prod_{\substack{++,+-,\\-+,--}} \left[\left(E_1\omega_1 \pm E_2\omega_2 \right)^2 - \left(\omega_1 \pm \omega_2 \right)^2 \right]$$

$$E(\omega_1, \omega_2, E_1, E_2) \equiv \left| \omega_1^4 \left(1+E_1^2\right)^3 - 2\omega_1^2\omega_2^2 \left(1+E_1^2\right)^2 \left(1-E_2^2\right) + \omega_2^4 \left(1-3E_1^2\right)\left(1+E_2^2\right) \right|$$

$$F(\omega_1, \omega_2, E_1, E_2) \equiv \left[\omega_1^4 \left(1+E_1^2\right)^3 - 2\omega_1^2\omega_2^2 \left(1+E_1^2\right)^2 \left(1-E_2^2\right) - \omega_2^4 \left(3-E_1^2\right)\left(1+E_2^2\right) \right]$$

References

[1] J.H. Taylor, “Bynary pulsars and relativistic gravity”, *Rev. of Mod. Phys*. **55** (1994) 551
[2] D.G. Blair et al, Phys. Rrev. Lett. 74 (1995) 1908-1911
[3] P. Astone et al., Phys. Rev. D 47 (1993) 362-365
[4] P. Astone et al., Astropart. Phys. 7 (1997) 231-243
[5] E. Mauceli et al., Phys. Rev. D 54 (1996) 1264
[6] M. Cerdonio et al., *Phis. Rev. Lett.* **71** (1993) 4107
[7] M. Cerdonio et al., *Phisica B* **194-196** (1994) 3-4
[8] Y. Ogawa, P. Rapagnani, “Lagrangian formalism for resonant capacitive transducers for gravitational-wave antennas”, *Nuovo Cimento **7C*** 1 (1984) 21
[9] S. Vitale et al., Fast numerical data analysis for resonant gravitational wave antennas and antennas arrays: optimal filtering, signal timing and internal vetoes, *Nucl. Phys.* **B48** (1996) 104-106
[10] V. Crivelli-Visconti et al., Timing with resonant gravitational wave detectors: an experimental test, *Phys. Rev. D* **57**,4 (1998) 2045-2050
[11] A. Papoulis, “Probability, random variables and stocastic processes”, McGraw-Hill, New York (1991)
[12] A. Papoulis, “Signal Analysis”, McGraw-Hill, New York (1977)
[13] W.W.S. Wei, Time series analysis: univariate and multivariate methods, Addison-wesley (1990)
[14] J.G. Proakis, D.G. Manolakis, “Digital signal processing principles, algorithms and applications”, Macmillan, New York (1988)
[15] W.H Press, S.A. Teukolsky, W.T. Vetterling, B.P. Flannery, “Numerical recipes in C: the art of scientific computing”, 2nd ed., Cambridge University Press (1992)
[16] Artifex is a CASE tool developed by “ARTIS”, http://www.artis.it/
[17] e.g.: G. Bruno, “Model-based software engineering”, Chapman and Hall, London (1995)
[18] C. Thomas, *Proc. of the IEEE* **79** (1991) 991
[19] ESAT s.r.l., via Brissogne,12 – 10142 Torino (Italy)
[20] H. Hilton, “10Msample/second ADC with filter and memory”, Hewlett-Packard Report; H. Hilton, 10MHz Adc with 110dB linearity, ibid.
[21] I.S. Heng and L. Baggio, in preparation
[22] A. Ortolan, “Realizzazione ed ottimizzazione di un osservatorio di onde gravitazionali”, PhD Thesis, Università degli Studi di Ferrara (1991)
[23] V. Martinucci, “Progettazione di una base dati relazionale per l’esperimento AURIGA”, Laurea Thesis, Università degli Studi di Padova (1998)
[24] Z.A. Allen et al, First search for gravitational wave bursts with a network of detectors, *Phys. Rev. Lett.* **85**, (2000) 5046-5050
[25] A. Ortolan, G. Vedovato, M. Cerdonio, S. Vitale, “Optimal reconstruction of the input signal in resonant gravitational wave detectors: data processing algoritms and physical limitations” *Phys. Rev D* **50** (1994) 4737
[26] S. Fantinel, , Laurea Thesis, Università degli Studi di Padova (2000)
[27] L. Baggio et al., Chi-square testing of optimal filters for gravitational wave signals: an experimental implementation, *Phys. Rev. D* **61** (2000) 102001-(1-9).
[28] L. Baggio et al., Fast data processing and on-line consistency tests with bars, in the proceeding of "Gravitational Wave Data Analysis Workshop (GWDAW-99)", Dec. 2-4, 1999, Roma, Italy, *Int. J. Mod. Phys. D* **9**, 251-255, 2000.
[29] G. A. Prodi et al., Initial operation of the International Gravitational Event Collaboration, in the proceeding of "Gravitational Wave Data Analysis Workshop (GWDAW-99)", Dec. 2-4, 1999, Roma, Italy, *Int. J. Mod. Phys. D* **9**, 237-245, 2000.
[30] L. Baggio et al., Bar detectors: present and future, in the proceeding of "The 2nd TAMA Workshop", (October 19-22, 1999, Tokyo, Japan) edited by S. Kawamura and N. Mio, Universal Academy Press, Tokyo (2000) 35-48.
[31] A. Ortolan et al., The logging and data retrieve system for the gw detector AURIGA, in "Gravitational waves", proceeding of the "Third Edoardo Amaldi Conference", (CalTech - California, 1999), edited by S.Meshkov, AIP Conference Proceedings, New York (2000) 471-472.
[32] L. Baggio et al., Resonant detectors for gravitational waves, presented at the "32nd COSPAR Scientific Assembly", July 12-19, 1998, Nagoya, Japan, published in *Adv. Space Res.* 25 (2000) 1171-1176.
[33] L. Baggio et al., The gravitational wave Burst Observatory: present state and future perspectives, *Nucl. Phys. B* (*Proc. Suppl*.) **70** (1999) 537-544
[34] M. Cerdonio et al., Cryogenic resonant detectors of gravitational waves: current operation and prospects, in "Gravitation and relativity: at the turn of the millennium", proceedings of the "GR-15 conference", (Pune - India, 1997), edited by N. Dadhich and J. Narlikar, IUCAA, Pune (1998) 211-230.

[35] G. A. Prodi et al., Initial operation of the gravitational wave detector AURIGA, in the proceedings of the "Second Edoardo Amaldi conference on gravitational wave experiments", (CERN - Switzerland, 1997), edited by E. Coccia, G. Veneziano, G. Pizzella, World Scientific, Singapore (1998) 148-158.
[36] A. Ortolan et al., "Data analysis for the resonant gravitational wave detector AURIGA: optimal filtering, χ^2 test, event timing and reconstruction", in the proceedings of the "Second Edoardo Amaldi conference on gravitational wave experiments", (CERN - Switzerland, 1997), edited by E. Coccia, G. Veneziano, G. Pizzella, World Scientific, Singapore (1998) 204-215.
[37] J-P. Zendri, in preparation
[38] S. Mukherjee and L.S. Finn, "Removing instrumental artifacts: suspension violin modes", proceeding of the "Third Edoardo Amaldi Conference", (CalTech - California, 1999), edited by S. Meshkov, AIP Conference Proceedings, New York (2000) 362-368